ELSEVIER

Journal of Structural Geology 27 (2005) 1986–2007

JOURNAL OF STRUCTURAL GEOLOGY

www.elsevier.com/locate/jsg

Strain state and kinematic evolution of a fold-nappe beneath the Samail Ophiolite, Oman

David R. Gray[a,*], John McL. Miller[a], Robert T. Gregory[b]

[a]*School of Earth Sciences, University of Melbourne, Melbourne, Vic. 3010, Australia*
[b]*Stable Isotope Laboratory, Department of Geological Science, SMU, Dallas, TX 75275, USA*

Received 13 August 2004; received in revised form 15 June 2005; accepted 28 June 2005
Available online 25 August 2005

Abstract

The Saih Hatat domal culmination of the Oman Mountains, Arabian Peninsula contains a major, refolded, NE-facing, recumbent, anticlinal fold-nappe within Pre-Ordovician sedimentary cover (autochthon) and Mesozoic platform carbonates that underlie the Samail and Hawasina nappes. Tracts of overturned stratigraphy covering over a 1000 km^2 are associated with a marked strain gradient towards sheath-like, a-type folds that define the fold-nappe lower limb transitional into an elongated SW-facing recumbent syncline and the underlying upper plate–lower plate shear zone. Directions of stretching recorded by fibrous, pressure shadow fringes on pyrite show a 20–30° counterclockwise rotation in the foliation plane. Strain and kinematic constraints require the fold-nappe to form progressively during top-to-the-NE shearing of the Arabian margin with (1) development of a high-strain zone, and (2) subsequent folding of the strongly deformed to transposed stratigraphy in the hanging wall to the shear zone. Rolling of the autochthonous stratigraphic layering of the upper limb through the hinge accompanied by differential shear strain produced the regional scale, highly attenuated a-type folds at the structurally lowest levels. This occurred by simple underthrusting of the footwall (lower plate), as the upper limb of the fold-nappe has to be pinned to the autochthon.

Keywords: Fold-nappe; Strain; Kinematics; Pressure shadows; a-Folds; Obduction; Oman

1. Introduction

Fold-nappes (after Bertrand, 1844) are kilometre-scale recumbent folds with hugely thinned and intensely deformed inverted limbs (Merle, 1998). The Helvetic and Pennine nappes of the European Alps are classic examples. It was argued that such structures evolved from overfolds or inclined, asymmetric fold pairs with a ductile zone/glideplane developing into an overthrust along the common limb (e.g. Heim, 1919–1922 in Merle, 1998). Many of the fold-nappes in the Alps, however, tend to emanate from root zones or regions of high strain involving both the basement and the sedimentary cover, with extrusion and movement towards the more external parts of the developing Alpine collisional orogen (e.g. Dietrich and Casey, 1989; Merle, 1998, fig. 52).

In NE Oman, on the Arabian Peninsula, a major regional-scale, fold-nappe occurs within platform carbonates beneath the Hawasina nappes and the obducted Samail Ophiolite thrust-nappe (Le Métour et al., 1986, 1990; see fig. 7 of Gregory et al., 1998; fig. 2 of Gray et al., 2000; fig. 2 of Miller et al., 2002). The question arises as to how and why such a major oceanwards-facing recumbent fold developed in the Arabian margin sequence late in the overthrusting, or just after the overthrusting of the ophiolite nappe.

To understand the process of nappe-formation, a detailed kinematic and strain study was undertaken by Gray, Miller and Gregory as part of regional structural mapping of NE Saih Hatat between 1994 and 1998. The investigation is similar to that undertaken on the Helvetic fold-nappes including the Morcle, Diableret and Wildhorn nappes by Durney (1972), Durney and Ramsay (1973), Dietrich and Durney (1986) and Dietrich and Casey (1989). Measurements were undertaken on all available strain markers including fibres in pressure shadows on pyrites in

* Corresponding author. Tel.: +61 3 8344 6931; fax: +61 3 8344 7761.
E-mail address: drgray@unimelb.edu.au (D.R. Gray).

0191-8141/$ - see front matter © 2005 Elsevier Ltd. All rights reserved.
doi:10.1016/j.jsg.2005.06.011

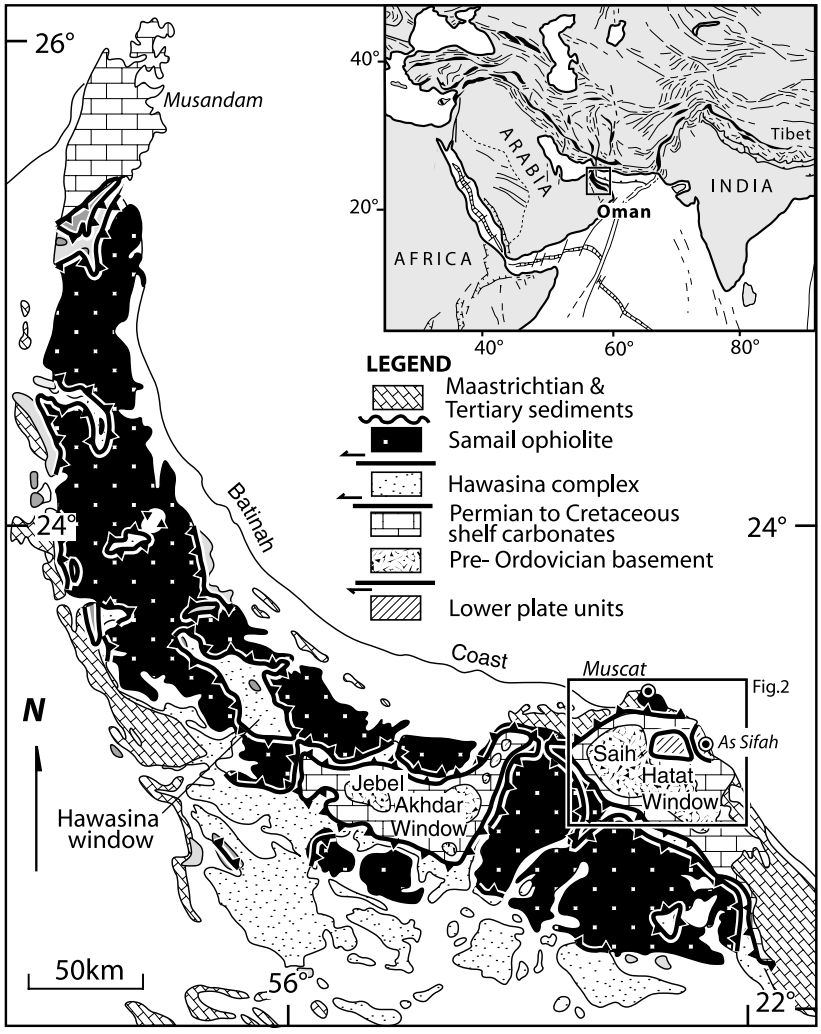

Fig. 1. Map of the Oman Mountains showing the outcrop distribution of the Samail Ophiolite and the location of the Saih Hatat domal culmination or window south of Muscat (modified from Glennie et al. (1974)). The coastal village of As Sifah marks the position of the deepest level rocks of the Oman Mountains. These rocks are partially retrogressed eclogites exposed in mega-boudins, as part of the lower plate of Gregory et al. (1998). Location of the map is shown in Fig. 2.

carbonates, mica schist and quartzite lithologies, conglomerate clasts in quartzite conglomerates, and amygdales, hyaloclastite fragments and pillows in mafic units. The results and interpretations of these data are presented in this paper, and a kinematic model for fold-nappe evolution discussed within the context of Samail Ophiolite obduction.

The development of the Saih Hatat fold-nappe represents some of the last stages in margin deformation (~76–70 Ma) during the obduction of the Samail ophiolite thrust-nappe. Dominated by an intense NE-directed shearing event, the strain and kinematic data preclude gravitationally induced spreading influences in Saih Hatat fold-nappe development, as well as the extruding mechanism of the Helvetic and Penninic nappes of the European Alps. The kinematic evolution outlined is analogous to oceanwards-directed overthrusting of the upper plate part of the margin in a tectonic wedge beneath a 'lid' of the ophiolite nappe, but there is a requirement of an active footwall or more simply underthrusting of the lower plate.

2. Background

2.1. The Oman Mountains

The Oman Mountains are dominated by the Samail Ophiolite nappe (Fig. 1), a large, now segmented slab of oceanic lithosphere that was emplaced onto the Arabian part of the northern Gondwana margin during closure of the southern NeoTethys ocean (Alleman and Peters, 1972; Glennie et al., 1974; Le Métour et al., 1990). Overthrusting of the Samail thrust-nappe has been considered to involve piggyback emplacement of successively outboard thrust slices including Permian–Mesozoic ocean floor and continental rise sediments (Hawasina units), which in turn overlie time equivalent Permian–Mesozoic shelf and slope facies carbonates (Hajar and Sumeini Groups; e.g. Searle, 1985; Lippard et al., 1986; Béchennec et al., 1990; Hanna, 1990; Mann and Hanna, 1990). This equates to

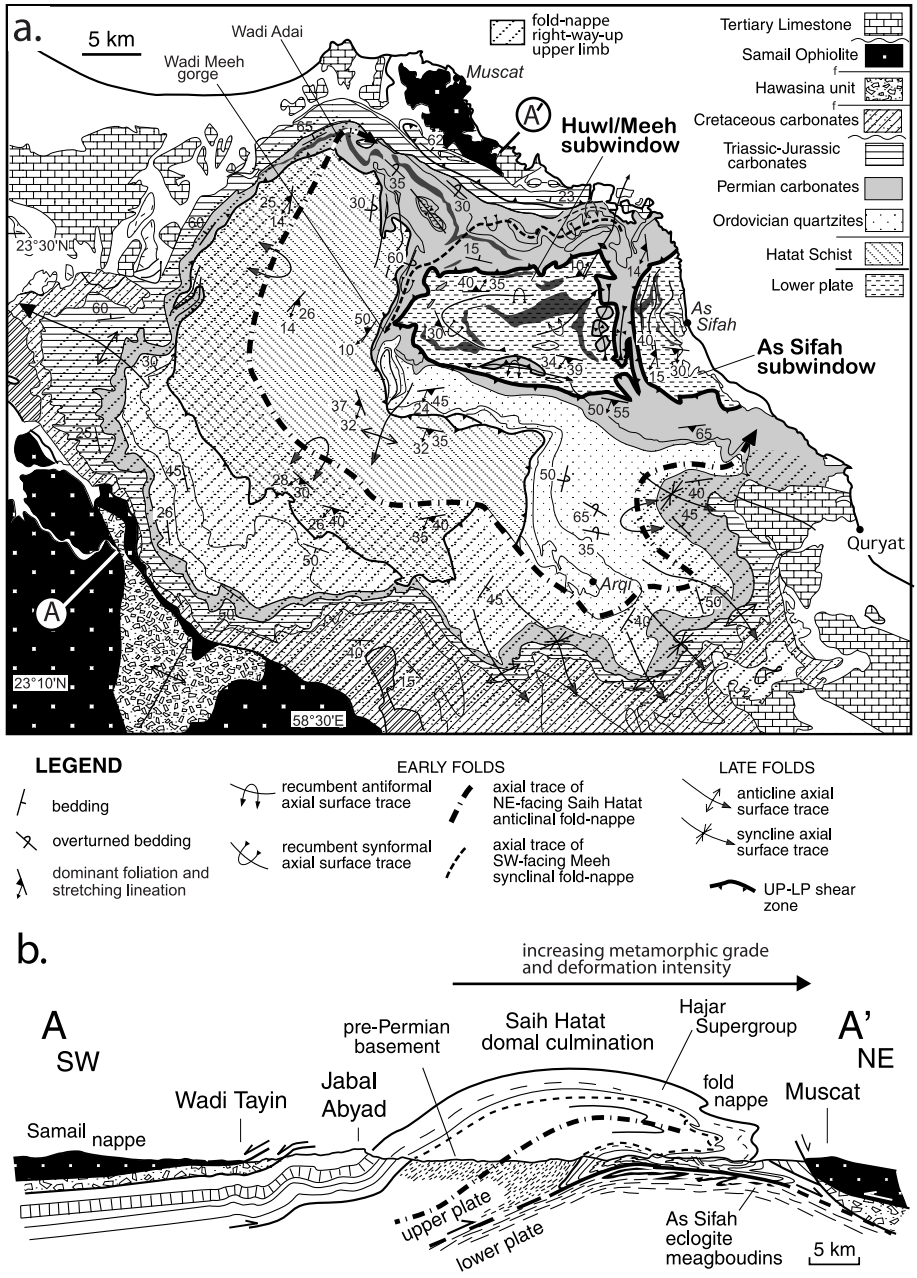

Fig. 2. (a) Map of the Saih Hatat domal culmination showing the axial surface trace of the Saih Hatat fold-nappe, as well as the distribution of the rightway-up limb (oblique slashed region), the UP–LP shear zone, the lower plate windows and the general distribution of major geological units (modified from Le Métour et al., 1986, 1990). The location of the profile in (b) is shown. (b) Regional structural profile of the Saih Hatat fold-nappe based on down- and up-plunge projection of the mapped region of northern Saih Hatat (see Miller et al., 2002). The NE increase in metamorphic grade and deformation intensity reflects structural thickening by the fold-nappe as well as proximity to the UP–LP shear zone (see text).

underthrusting-accretion beneath the Samail Ophiolite with stacking of distal to proximal units.

Tertiary deformation of the mountain range has produced a series of domal culminations within the overlying Samail Ophiolite nappe sheet (Glennie et al., 1974; Mount et al., 1998), represented by the Hawasina, Jabal Akhdar and Saih Hatat windows, respectively (Fig. 1). These domal culminations provide a window beneath the ophiolite nappe and a view of how the margin behaved during the obduction of the ophiolite (e.g. Gray and Gregory, 2003).

2.2. The Saih Hatat domal culmination

The eroded, L-shaped Saih Hatat domal culmination (Figs. 2 and 3) is the easternmost window of the Samail Ophiolite thrust sheet (Fig. 1). The domal culmination is cored by recessively weathered Pre-Ordovician Hatat Schist and rimmed largely by Permian and Triassic carbonates (Fig. 3). The presence of the culmination has been linked to inferred, but yet unproven subsurface thrust ramps (e.g. Searle, 1985; Goffé et al., 1988; Hanna, 1990; Cawood

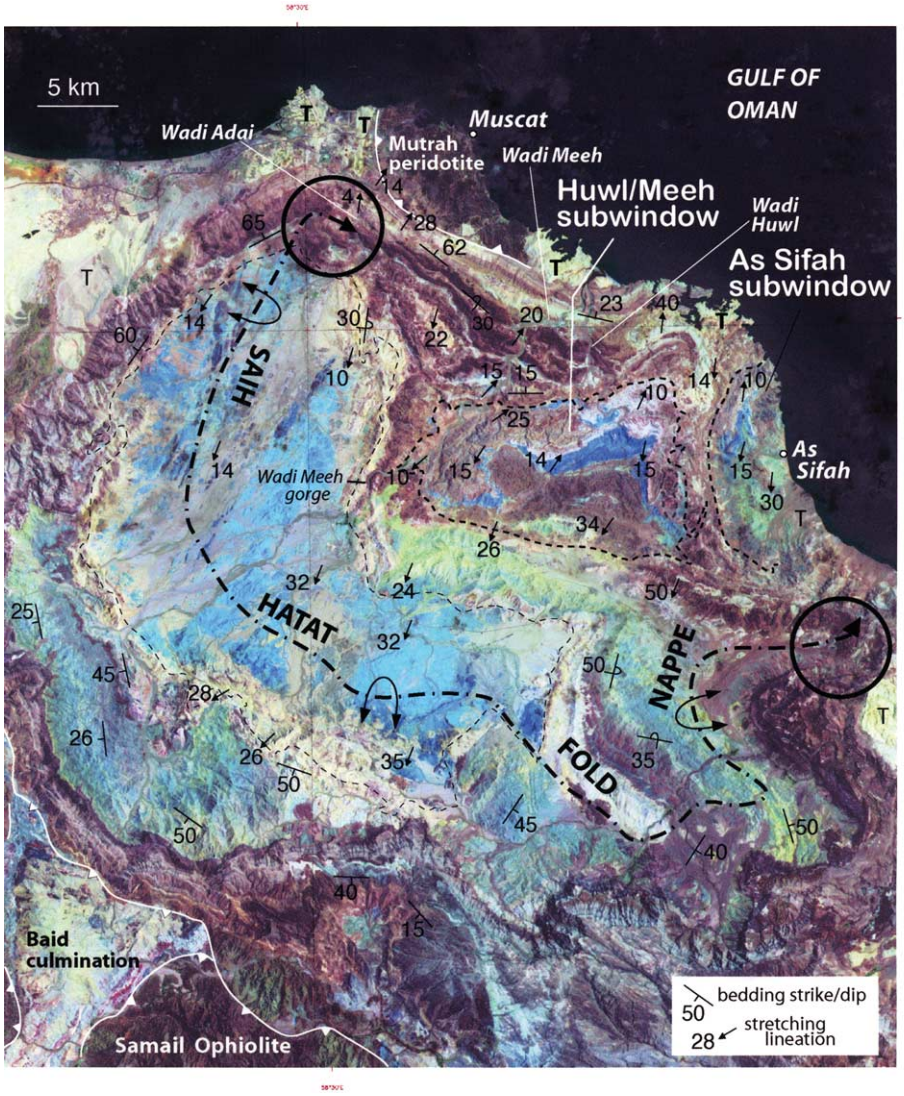

Fig. 3. False colour Landsat 5 satellite image of the Saih Hatat domal culmination of NE Oman. The band ratios highlight the mafic units in blue and the carbonates in darker shades of brown. The axial surface trace of the Saih Hatat fold-nappe is shown as well as the trace (dashed lines) of the UP–LP shear zone defining the Huwl and As Sifah windows. Compare with the geological map of Fig. 2a. The circled regions define the cliff and/or hillside exposures of the hinge zone of the Saih Hatat fold-nappe. Some lineation data (plunge and plunge direction) and the attitudes of bedding (strike and dip) are shown. T, Maastrichtian–Tertiary limestones.

et al., 1990) or thick-skinned reverse faults (e.g. Mount et al., 1998). The L-shaped form of the window relates to fold interference between the NE-facing Saih Hatat fold-nappe (Fig. 2) and later overprinting Maastrichtian or Tertiary sets of interfering N–S-, NW–SE-, NNE-trending folds (Fig. 4; Miller et al., 2002).

The core of the domal culmination coincides with the core of the major Saih Hatat fold-nappe (Fig. 2), and contains strongly deformed, pre-Ordovician Hatat Schist that forms basement to the platform upper plate shelf carbonates. The Hatat Schist shows transposition layering and a well-developed lineation that parallels the regional Cretaceous lineation (cf. Michard et al., 1984).

The structurally lowest parts within the Saih Hatat domal culmination are not these Pre-Ordovician units, but intensely deformed quartz-mica schist, mafic schist and calc schist below a major, crustal-scale shear zone that separates the region into upper and lower plates (see Fig. 2b; Gregory et al., 1998; Miller et al., 1998, 2002; Gray et al., 2000). These transposed and recumbently folded schist units (e.g. Miller et al., 2002; Gray et al., 2004a,b) occur in lower plate exposures of the Hulw and As Sifah windows, essentially subwindows in the northeast part of the culmination (Fig. 2a). Eclogites occur within mafic boudins (El-Shazly and Coleman, 1990; Searle et al., 1994, 2004; Miller et al., 1998, 1999, 2002; Gray et al., 2004a,b) in the easternmost exposure of the As Sifah lower plate window and represent the deepest exposed levels of the Oman Mountains.

Across the domal culmination to the NE, there is an apparent increase in strain, deformation intensity and

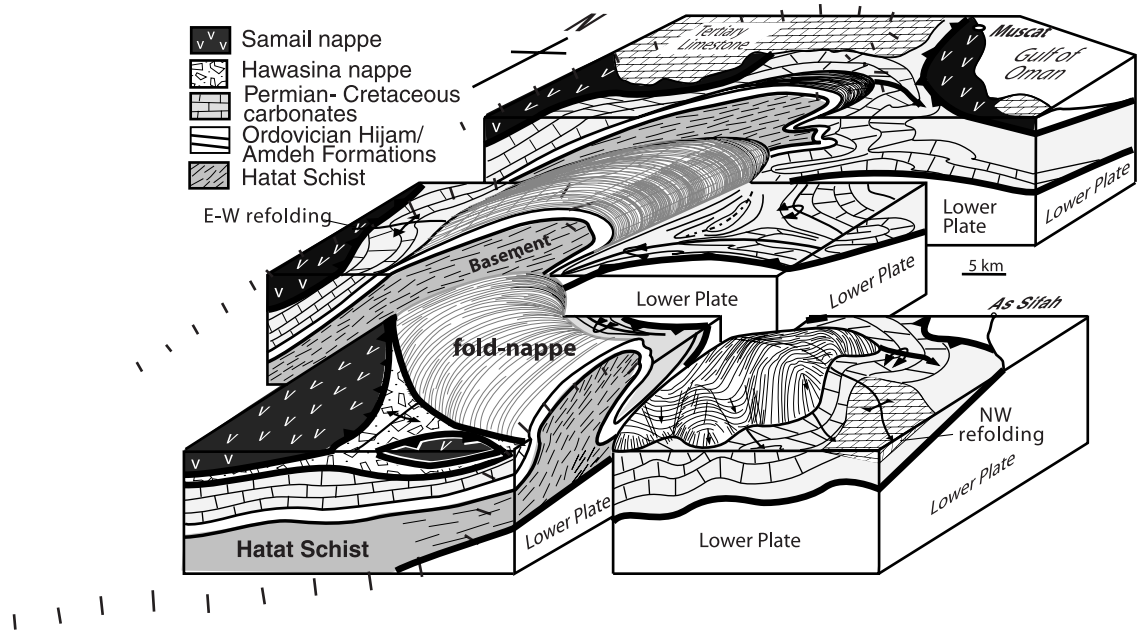

Fig. 4. Block diagram of the map region of Fig. 2a broken into four blocks to illustrate the 3D form of the Saih Hatat fold-nappe within the Saih Hatat domal culmination. The locations of Muscat and As Sifah are shown in the map view. The core of the fold-nappe is intensely deformed Hatat Schist (the 'basement' to the Permo-Cretaceous carbonate shelf).

metamorphic grade (Le Métour et al., 1986, 1990; Miller et al., 1998, 2002). The deformation gradient is shown by strong fabric (L–S tectonite) development resulting in a pervasive schistosity and regional fold-nappes that have isoclinal, sheath-like fold geometry and markedly thinned or attenuated stratigraphy along fold limbs (Le Métour et al., 1986, 1990; Miller et al., 2002; Breton et al., 2004). The apparent increase in deformation intensity coincides with the hinge zone and lower limb of the Saih Hatat fold-nappe, as well as the underlying major crustal shear zone (the upper plate–lower plate discontinuity of Gregory et al., 1998) and lower plate schist units exposed in the NE part of the domal culmination (Fig. 2).

3. Geometry of the Saih Hatat fold-nappe

The three-dimensional form of the Saih Hatat fold-nappe

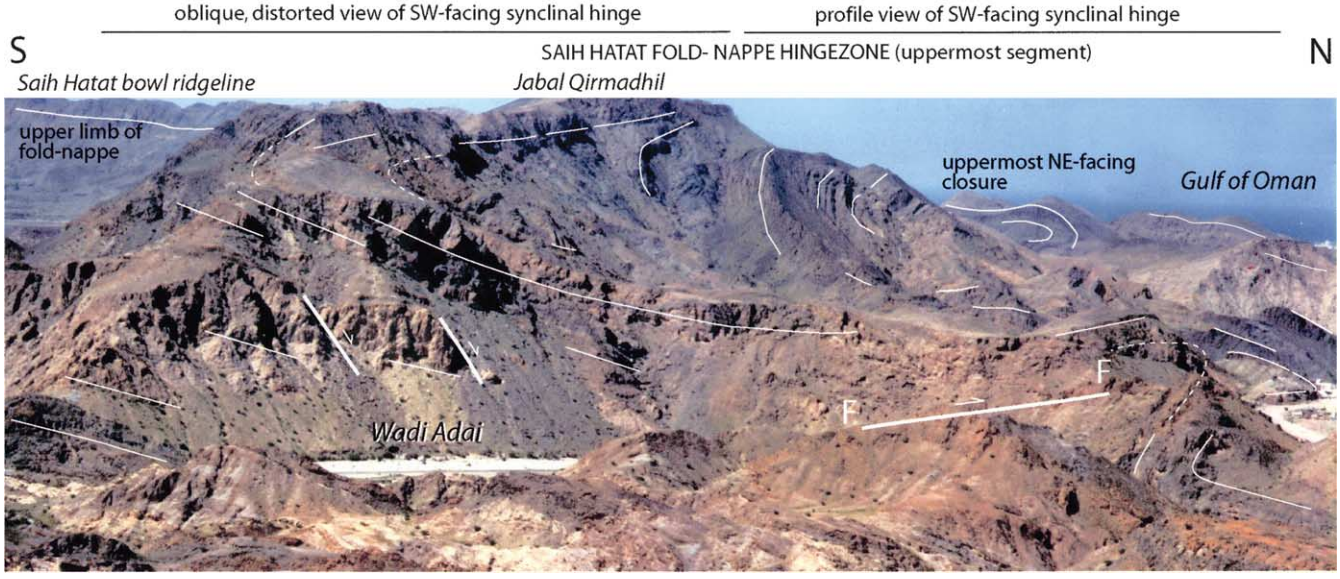

Fig. 5. Photographic collage of Jabal Qirmadhil showing the upper folds within the hinge zone of the Saih Hatat fold-nappe. The view is looking northwest (330°) from a hill on the east side of Wadi Adai (UTM 40Q: 2603851/657167). The photograph was taken prior to construction of the Wadi Adai dual-carriageway freeway.

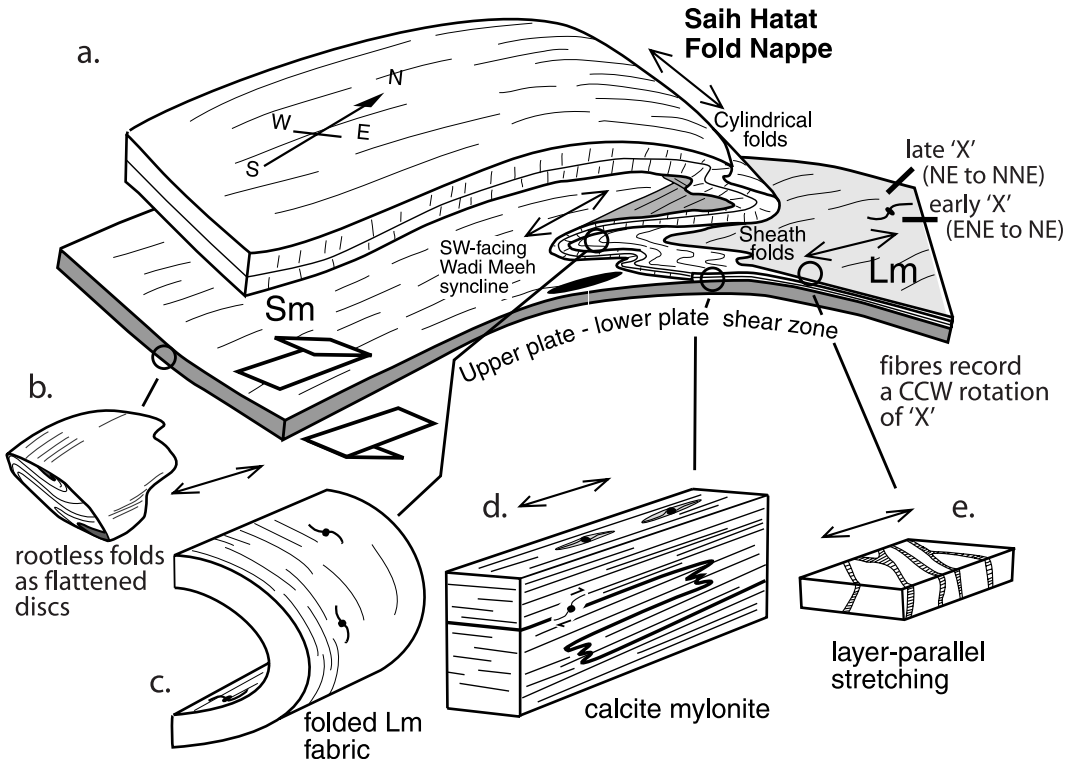

Fig. 6. Upper plate geometry and kinematic indicators of the Saih Hatat fold-nappe. Diagram is modified from fig. 3 of Miller et al. (2002). Black circles and ellipses represent strain markers. Structures and kinematic indicators are (b) disc-like flattened rootless hinges of asymmetric fold pairs that occur in the high-strain UP–LP shear zone and lower plate beneath the UP–LP shear zone. Based on structures in Wadi Huwl; (c) folded Lm fabric and pressure fringes based on folds in Wadi Meeh gorge; (d) flattened and attenuated chevron folds in calcite mylonite based on examples in side wadi off Wadi Meeh north of Al Hammah; (e) filigree pull-apart structure with fibrous veins typical of strongly deformed, thinly bedded Saiq 3 limestones. Based on structures in the Yiti region, north end of Wadi Meeh.

is a banana-shaped NE-facing and closing major anticlinal recumbent fold (Fig. 4) that is hidden in map view by the dominant outcrop traces of the ovoid-shaped Saih Hatat domal culmination; the form and presence of the Saih Hatat fold-nappe are not readily apparent on Landsat imagery of the domal culmination (Fig. 3). This is due to the low angle intersection between the present topography and the largely flat-lying limbs and fold axial surfaces, related to the recumbent form of the structure (see Fig. 2b).

Furthermore, only parts of the larger-scale structure are

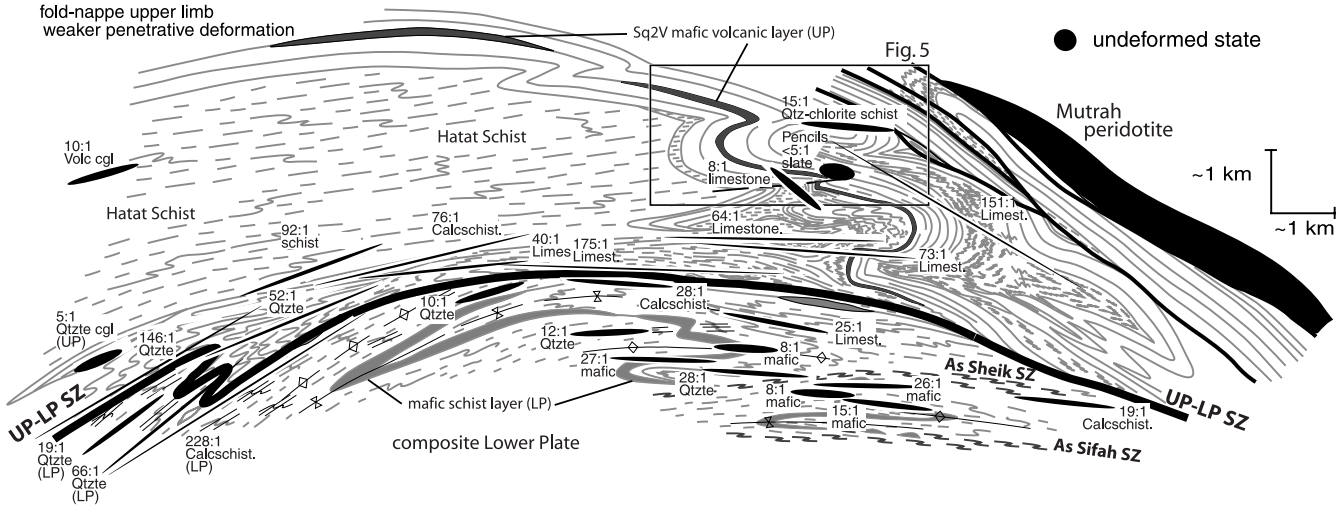

Fig. 7. Composite down-plunge and up-plunge profile of the major, NE-facing and closing Saih Hatat fold-nappe (based on Miller et al., 2002). *XZ* strain ellipses (where *X* and *Z* are the maximum and minimum principal stretches, respectively) are shown based on strain data presented in this paper (see Tables 1 and 2). The box outlines the region of the photograph in Fig. 5.

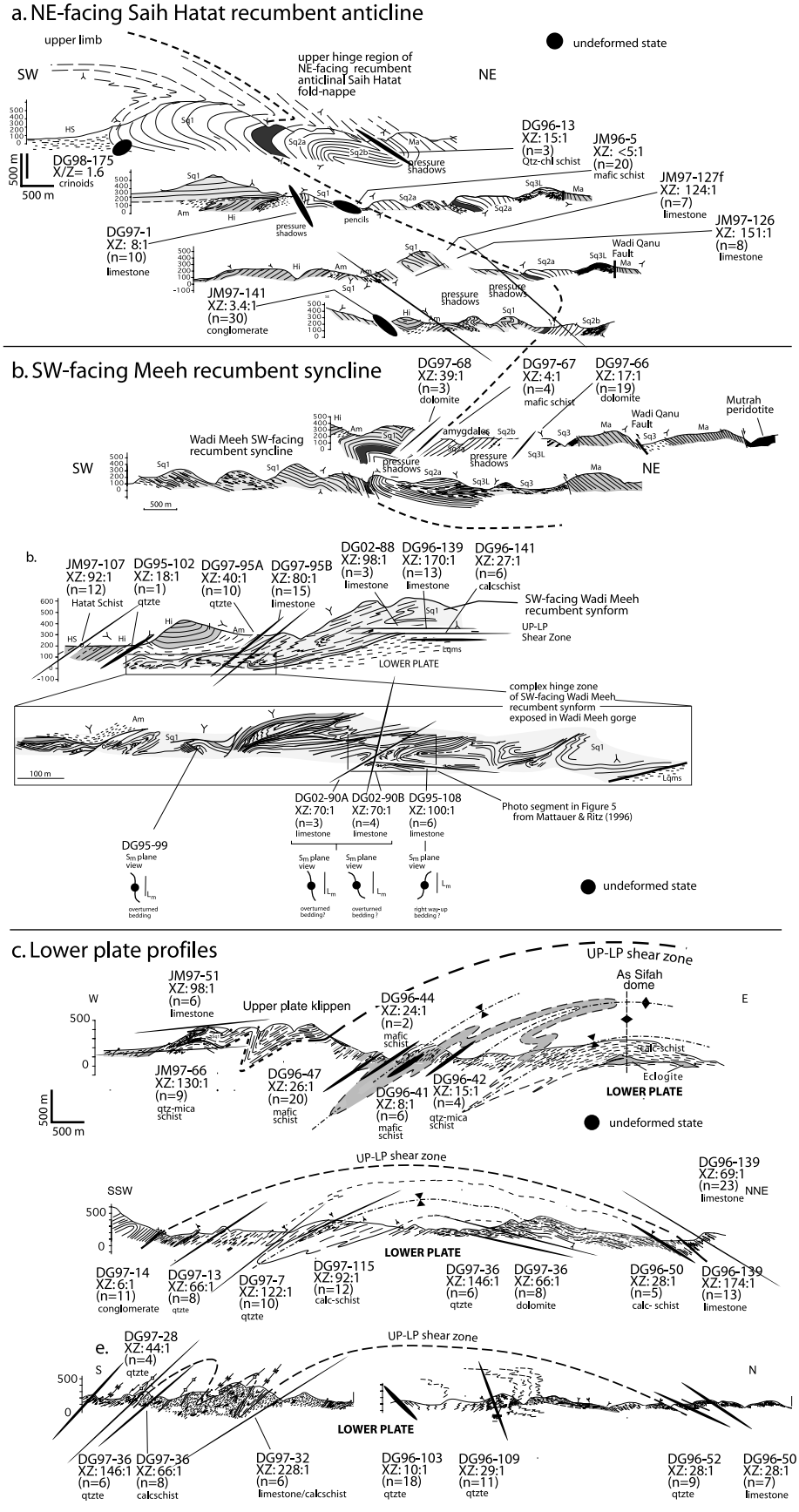
a. NE-facing Saih Hatat recumbent anticline
upper limb
undeformed state
SW
upper hinge region of NE-facing recumbent anticlinal Saih Hatat fold-nappe
NE
DG96-13 XZ: 15:1 (n=3) Qtz-chl schist
JM96-5 XZ: <5:1 (n=20) mafic schist
DG98-175 X/Z= 1.6 crinoids
JM97-127f XZ: 124:1 (n=7) limestone
JM97-126 XZ: 151:1 (n=8) limestone
DG97-1 XZ: 8:1 (n=10) limestone
Wadi Qanu Fault
JM97-141 XZ: 3.4:1 (n=30) conglomerate
pressure shadows
pencils
b. SW-facing Meeh recumbent syncline
DG97-68 XZ: 39:1 (n=3) dolomite
DG97-67 XZ: 4:1 (n=4) mafic schist
DG97-66 XZ: 17:1 (n=19) dolomite
Mutrah peridotite
Wadi Meeh SW-facing recumbent syncline
amygdaloid
SW
NE
b.
JM97-107 XZ: 92:1 (n=12) Hatat Schist
DG95-102 XZ: 18:1 (n=1) qtzte
DG97-95A XZ: 40:1 (n=10) qtzte
DG97-95B XZ: 80:1 (n=15) limestone
DG02-88 XZ: 98:1 (n=3) limestone
DG96-139 XZ: 170:1 (n=13) limestone
DG96-141 XZ: 27:1 (n=6) calcschist
SW-facing Wadi Meeh recumbent synform
UP-LP Shear Zone
LOWER PLATE
complex hinge zone of SW-facing Wadi Meeh recumbent synform exposed in Wadi Meeh gorge
DG02-90A XZ: 70:1 (n=3) limestone
DG02-90B XZ: 70:1 (n=4) limestone
DG95-108 XZ: 100:1 (n=6) limestone
Photo segment in Figure 5 from Mattauer & Ritz (1996)
DG95-99
overturned bedding
overturned bedding?
overturned bedding ?
right way-up bedding ?
undeformed state
c. Lower plate profiles
UP-LP shear zone
As Sifah dome
W
E
JM97-51 XZ: 98:1 (n=6) limestone
Upper plate klippen
DG96-44 XZ: 24:1 (n=2) mafic schist
calc-schist
Eclogite
LOWER PLATE
JM97-66 XZ: 130:1 (n=9) qtz-mica schist
DG96-47 XZ: 26:1 (n=20) mafic schist
DG96-41 XZ: 8:1 (n=6) mafic schist
DG96-42 XZ: 15:1 (n=4) qtz-mica schist
undeformed state
SSW
NNE
DG96-139 XZ: 69:1 (n=23) limestone
DG97-14 XZ: 6:1 (n=11) conglomerate
DG97-13 XZ: 66:1 (n=8) qtzte
DG97-7 XZ: 122:1 (n=10) qtzte
DG97-115 XZ: 92:1 (n=12) calc-schist
DG97-36 XZ: 146:1 (n=6) qtzte
DG97-36 XZ: 66:1 (n=8) dolomite
DG96-50 XZ: 28:1 (n=5) calc- schist
DG96-139 XZ: 174:1 (n=13) limestone
e.
DG97-28 XZ: 44:1 (n=4) qtzte
S
N
DG97-36 XZ: 146:1 (n=6) qtzte
DG97-36 XZ: 66:1 (n=8) calcschist
DG97-32 XZ: 228:1 (n=6) limestone/calcschist
DG96-103 XZ: 10:1 (n=18) qtzte
DG96-109 XZ: 29:1 (n=11) qtzte
DG96-52 XZ: 28:1 (n=9) qtzte
DG96-50 XZ: 28:1 (n=7) limestone

visible in the cliff exposures of the wadi walls (e.g. Wadis Adai, Meeh and Huwl; see Fig. 3). As a consequence, the regional-scale fold-nappe has not been recognised by other workers and is therefore not shown in profiles across the dome (e.g. fig. 3 of Mount et al., 1998; see also summary fig. 7 of Gray and Gregory, 2003). A clue as to its presence is shown by the region of 100 km^2 of overturned bedding in the NE part of the dome (see fig. 8 of Miller et al., 2002), originally identified by Glennie et al. (1974), Bailey (1981) and Le Métour et al. (1986). This overturned section is part of the common limb between a regional, northeast-facing anticlinal fold-nappe, exposed in the hills above Wadi Adai (Fig. 5) and a large, SW-facing synclinal recumbent isocline exposed in Wadi Meeh (Figs. 6 and 7).

In profile, the Saih Hatat fold-nappe has a distinct flat-topped, porpoise-like or bulbous form closing to the NE (Fig. 7), but in map view it has a crescentic shape due to refolding by fold interference that formed the Saih Hatat domal culmination (Fig. 4). The major closures that define the hinge zone of the anticlinal closure (Fig. 8a) are only visible in Jabal Qirmadihl above Wadi Adai (Fig. 5) in the NW corner of the dome and in the cliff-forming wall defining the valley in the central-east part of the dome (circled regions in Fig. 3).

The upper limb of the fold-nappe is represented by the southwest side of the present dome (region with oblique slash pattern in Fig. 2a) and consists of weakly to moderately deformed Permian to Cretaceous carbonates of the autochthon. The lower overturned limb of the Saih Hatat fold-nappe occurs on the northeast side of the Saih Hatat domal culmination, and therefore has inverted stratigraphy and is isoclinally folded and intensely deformed.

The overall geometry of the fold-nappe, structural style and some of the kinematic indicators are shown in Fig. 6. In the uppermost NE-facing recumbent anticlinal hinge (Fig. 8a), the major folds (exposed in Jabal Qirmadhil; Fig. 5) tend to be more cylindrical and have hingelines orthogonal to the NE-trending stretching lineation (Fig. 6a). The structurally lower, recumbent SW-facing Wadi Meeh syncline (Fig. 8b), exposed in hills on the north side above Wadi Meeh (Fig. 3 for location), is oriented sub-parallel to the stretching lineation (Fig. 6) and shows higher strains, more attenuated stratigraphy, sheath-like minor folds (cf. Mattauer and Ritz, 1996) and a general bulbous form within the Saiq limestones (Fig. 7). The major hinge in Saiq 1 limestones (Fig. 8b), exposed in Wadi Meeh gorge, consists of a complex zone of recumbent, sheath-like folds (cf. Mattauer and Ritz, 1996; Miller et al., 2002).

The lower limb of the Wadi Meeh syncline is markedly thinned with calcite mylonites in Saiq 1 and 2 limestones (Fig. 6d) and *chocolat du tablat* structures in the thin-bedded Saiq 3 limestones (Fig. 6e). This attenuated stratigraphy of the lower limb dips to the NE and is truncated against the upper plate–lower plate shear zone (Fig. 9e). Hanging wall stratigraphic cutoffs young to the NE (see Fig. 9e) indicating that a proto-shear zone responsible for the stratigraphic offset and the observed stratigraphic cutoffs could not have dipped oceanwards (see Fig. 9b and d) as required by simple overthrusting models (e.g. Searle et al., 1994, 2004; Searle and Cox, 1999).

4. Metamorphic conditions of fold-nappe development

Upper plate peak assemblages associated with the Saih Hatat fold-nappe are distinguished by the presence of carpholite, lawsonite and sodic amphibole without garnet (e.g. Goffé et al., 1988; El Shazly, 1994, 1995; Miller et al., 1998). Estimated *P–T* conditions range from:

- 6.8–9 kbar and 315–435 °C (El-Shazly, 1994, 1995) based on the absence of aragonite and the inferred stability fields of magnesio-carpholite, ferro-carpholite and chloritoid.
- −8–10 kbar and 180–250 °C (Goffé et al., 1988) based on carpholite–kaolinite assemblages.
- 6–8 kbar and 250–350 °C (Goffé et al., 1988) based on Fe/Mg carpholite–pyrophyllite assemblages.

Microstructural relationships after Goffé et al. (1988) and Michard et al. (1984, 1994) indicate that the high-*P* metamorphism in the upper plate predates the development of the dominant fabric in these rocks. This is shown by radiating ferrocarpholite phenoblasts in Jurassic Sahtan carbonates (Wadi Adai valley) that are boudinaged and enveloped by the dominant foliation (see fig. 6 of Michard et al., 1994) and contact strain effects about radiating Fe–Mg carpholite neoblasts by the overprinting and enveloping dominant foliation in Ruwi limestones (see fig. 10 of Michard et al., 1984).

5. Timing of fold-nappe development

Phengites defining the axial surface foliation to the Saih Hatat upper plate fold-nappe have yielded a 70.0 ± 0.7 Ma $^{40}Ar/^{39}Ar$ crystallization age (see sample JM96-93L, fig. 8f of Miller et al., 1999), whereas micas defining the NE-trending lineation in strongly deformed limestone in the immediate hanging wall to the UP–LP shear zone have yielded an age of 75.7 ± 0.6 Ma (see sample JM96-31b-L,

Fig. 8. Series of structural profiles across selected parts of NE Saih Hatat (for locations and more detail see Miller et al. (2002)). *XZ* strain ellipses in black with station, strain ratio, sample size (*n*) and lithology shown for each strain sampling locality. (a) Series of stacked profiles between Jabal Qirmadhil in the north and the north end of Wadi Meeh in the south. These show the geometry of the folds that define the hinge zone of the NE facing, major Saih Hatat fold-nappe in the north of the domal culmination. Form lines following the Saiq 2V volcanic member (black layer) define the structure. (b) Structural profiles for the Wadi Meeh synformal SW-facing closure. (c) Structural profiles across the As Sifah and Huwl lower plate windows.

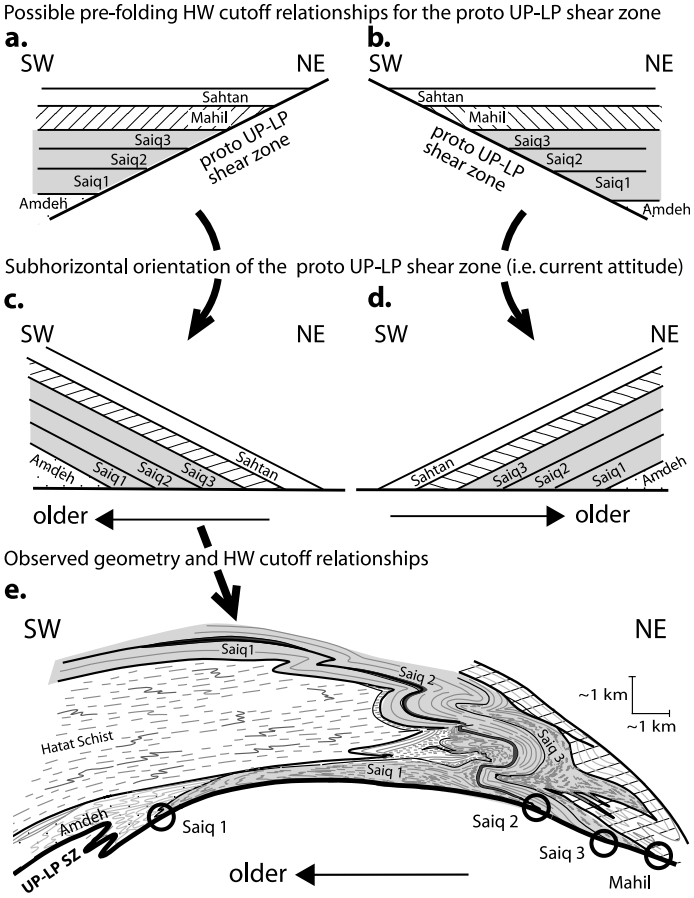

Fig. 9. Hanging wall stratigraphic cut-off diagrams constructed to establish the geometry of the proto UP–LP plate shear zone prior to fold-nappe development and the later doming. (a) and (b) Schematic hanging wall cut-off diagrams for SW- and NE-dipping proto-shear zone scenarios, respectively. (c) and (d) The proto-shear zones depicted in (a) and (b) rotated to the horizontal to approximate the present subhorizontal attitude shown in (e). (e) Saih Hatat fold-nappe profile with circles marking the hanging wall cut-offs against the UP–LP shear zone for the Amdeh/Saiq 1 contact, the Saiq 1/Saiq 2 contact, the Saiq 2/ Saiq 3 contact and the Saiq 3/Sahtan contact. Note the observed stratigraphic cut-off relationships match those in (c) indicating that the shear zone did not dip toward the NE or former ocean as required in the simple overthrusting model for obduction.

fig. 8e of Miller et al., 1998). Quartz–mica schist from the lower plate just below the UP–LP shear zone at the same locality displays an age gradient progressively increasing from ~74 Ma to a plateau age of 91.0±1.4 Ma (52% of gas; see sample JM96-32a, fig. 7f of Miller et al., 1999), again suggesting UP–LP shear zone activity at ~76–74 Ma.

The upper plate folding therefore postdates the proto-UP–LP shear zone, as dominant mica fabrics from the lower plate shear zones yield $^{40}Ar/^{39}Ar$ phengite ages of 82–79 Ma (Miller et al., 1999; Gray et al., 2004a,b). The upper plate shows a marked strain gradient towards the UP–LP shear zone, which indicates that this shear zone continued to operate at the time of Saih Hatat fold-nappe development. The supporting $^{40}Ar/^{39}Ar$ geochronology indicates that mica growth synchronous with upper plate nappe formation was from 76 to 70 Ma (Miller et al., 1998).

6. Total strain markers

Strain markers are predominantly pressure shadows in limestone, dolomite, mica schist, quartzite and mafic schist layers (Fig. 10), pulled apart layers, deformed fossils (e.g. crinoids and ammonites), conglomerate clasts, and amygdales, hyaloclastite fragments and pillows in mafic volcanics (Table 1).

6.1. Strain state

The defined strain states determined from all measured available total strain markers, apart from pressure shadows, cover a wide spectrum (Fig. 11) with shape factors specified by Flinn k values ranging between 5.0 (constrictional field) and 0.25 (field of apparent flattening), where $k=(a-1)/(b-1)$ for $a=(e_1+1)/(e_2+1)$ and $b=(e_2+1)/(e_3+1)$ after Flinn (1962). In terms of Nadai octahedral shear strain (ε_s), the data range between 0.75 and 1.75, where ε_s is after Nadai (1963, p. 73). More than 50% of the data plot between ε_s values of 1.25 and 0.75 (Fig. 11).

Measured marker shapes (Fig. 11) include flattened cigars (constriction field) to elongate discs (flattening field). The different measured shapes reflect initial shape

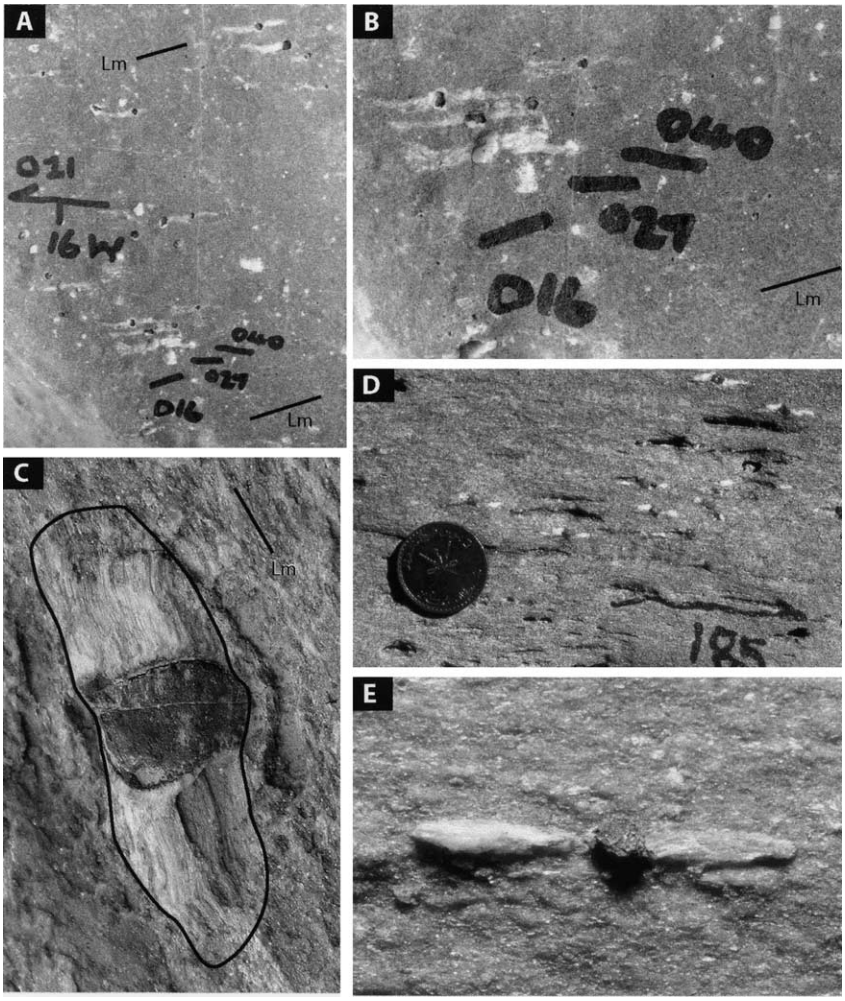

Fig. 10. Photographs of pressure shadows in NE Saih Hatat. All are views of the foliation Sm surface or *XY* plane, apart from (D) which is a view normal to the foliation in a plane containing the lineation, i.e. the *XZ* or movement plane; where *X*, *Y* and *Z* are the maximum, intermediate and minimum principal stretches, respectively. (A) Curved pressure shadow fringe on pyrite in Saiq 1 limestones, Wadi Meeh gorge. Base of photo is ~8 cm. Lm denotes the stretching lineation. (B) Enlargement of part of (A) showing detail of the fibres with orientation changes. Base of photo is ~5 cm. (C) Large pressure shadow with fibrous quartz fringes showing a complex growth increments in overturned Amdeh mica quartzite, Wadi Meeh gorge. Base of photo is 4 cm. (D) Curved fibrous pressure shadow fringes on euhedral pyrites in mafic schist, southern Huwl window. Fibre curvature indicates top-to-the-NNE shear sense. Coin diameter is 2.3 cm. (E) Partially recrystallised drawn-out formerly fibrous pressure shadow fringes in calcite mylonite (JM97-108), Wadi Meeh gorge. Base of photo is 3 cm.

variations between the markers, as well as the superimposed total strain state. Pillows in the mafic schists would have initial ellipsoidal forms, while the hyaloclastites are inferred to have been more irregular, with plate-like initial shapes. In contrast, amygdales would have had the closest to an initial spherical shape. A mafic schist locality in the upper plate (e.g. DG97-67) contained both carbonate–chlorite amygdales and glassy fragments. At this locality, the amygdales indicated a plane strain deformation, whereas the glassy fragments record an apparent flattening deformation close to plane strain ($k=0.6$) (Fig. 11).

Quartzite clasts in quartzite-dominated conglomerates, which mainly occur in the Amdeh unit in the upper plate (Fig. 12a), show a variety of strain states and strain magnitudes (Fig. 11). The highest *XZ* strains are from markers with flattened cigar shapes plotting in the constrictional field (DG97-50, Fig. 11).

The variation in strain state (i.e. constrictional versus flattening components) has to be real as shown by amygdales in the mafic volcanics, which must have had an initial spherical shape. Amygdales either plot close to plane strain (DG97-67, Fig. 11) or within the field of apparent constriction (DG96-124 with a Flinn $k=5$; Fig. 11).

Ductility differences are highlighted by different shape factors for calcite versus quartz-albite amygdales from the same locality (DG96-124; Fig. 11); both have Flinn *k* values of 4.3 and 5.1, respectively, but significant variation in the natural strain with values of ~0.8 and ~1.35.

Table 1
Total strain data—Saih Hatat

Station	Marker	Location	Coordinates	Lithology	*n*	*X*/*Y*	*Y*/*Z*	*X*:*Y*:*Z*	*k*
DG96-3	Pencil structure	Upper plate, Wadi Adai	40Q 260519/65654	Siltstone	22	1.1	1.1	1.1:1:0.9	1.0
JM96-5C	Pencil structure	Upper plate, Wadi Adai	40Q 260519/65654	Siltstone	13	1.1	1.1	1.1:1:0.9	1.0
DG96-63	Pillows	Huwl lower plate	40Q 2596440/669120	Mafic schist	9	2.4	1.5	2.4:1:08	2.8
DG96-78	Chlorite amygdales	Huwl lower plate	40Q 2592940/669220	Mafic schist	8	2.1	3.1	2.1:1:0.32	0.5
DG96-90	Pillows	Huwl lower plate	40Q 2593570/673985	Mafic schist	7	2.54			
DG96-92	Hyaloclastite fragments	Huwl lower plate	40Q 2591995/672845	Mafic schist	9	2.3	3.2	2.3:1:0.31 0.6	
DG96-113	Amygdales	Huwl lower plate	40Q 2593501/669345	Mafic schist	6	1.7	3.9	1.7:1:0.26	0.2
DG96-124	Calcite amygdales	Huwl lower plate	40Q 258925/67394	Mafic schist	9	2.3	1.3	2.3:1:0.77	4.3
DG96-124	Quartz-albite amygdales	Huwl lower plate	40Q 258925/67394	Mafic schist	9	3.8	1.6	3.8:1:0.64	4.7
DG96-157	Pebble conglomerate	Upper plate near, Al Khufayqi	40Q 2589290/657245	Quartzite	12	2.2	1.6	2.2:1:0.64	2.0
DG97-5	Stretched tourmaline	Huwl lower plate, Wadi Shakari	40Q 259082/66678	Quartzite	4	1.8			
DG97-14	Pebble conglomerate	Huwl lower plate	40Q 258798/66336	Quartzite	11	2.5	5.6	2.5:1:0.45	0.3
DG97-18	Ellipsoidal pulled-apart pyrites	Upper plate, near Al Afiah	40Q 258601/67178	Quartzite	7	4.7	2.3	4.7:1:0.43	2.8
DG97-19	Pebble conglomerate	Upper plate, near Al Afiah	40Q 258584/67372	Quartzite	11	2.4	2.6	2.4:1:0.38	0.9
DG97-23	Ammonites	Huwl lower plate	40Q 2587409/669395	Limestone	6	1.4	2	1.4:1:0.50	0.4
DG97-50	Pebble conglomerate	Upper plate	40Q 2585647/658186	Platy quartzite	10	4.5	2.2	4.5:1:0.46	2.9
DG97-55	Stretched dolomite pod	Upper plate, near Hammah	40Q 258503/672780	Quartzite	1	1.5			
DG97-55	Dolomite blebs	Upper plate, near Hammah	40Q 258503/672780	Quartzite	10	3			
DG97-57	Pebble conglomerate	Upper plate, near Al Afiah	40Q 258368/675077	Platy quartzite	5	3.7	3.7	3.7:1:0.27	1.0
DG97-59	Pebble conglomerate	Upper plate, near Hayfadh	40Q 258245/675300	Quartzite	5	1.1			
DG97-64	Pelloidal shapes	Upper plate, W of Wadi Meeh	40Q 2602308/664165	Limestone	10	2.3			
DG97-67	Chlorite-calcite amygdales	Upper plate, W of Wadi Meeh	40Q 2601570/661719	Mafic volcanic	9	2	2	2.0:1:0.50	1.0
DG97-67	Pumiceous mafic volcanic	Upper plate, W of Wadi Meeh	40Q 2601570/661719	Mafic volcanic	13	2.9	4.2	2.9:1:0.24	0.6
DG97-67	Hyaloclastite	Upper plate, W of Wadi Meeh	40Q 2601570/661719	Mafic volcanic	5	2.5	3.4	2.5:1:0.29	0.6
DG98-02	Pulled apart pyritic nodule	Upper plate, near Al Afiah	40Q 2581530/664740	Quartzite	1	1.3			
DG98-109	Pebble conglomerate	Upper plate, Arqi	40Q 2569880/673544	Quartzite	16	1.6	3	1.6:1:0.33	0.3
DG98-115	Stretched pyrite	Upper plate, southern Saih Hatat	40Q 2583669/665176	Quartzite	4	2.1			
DG98-118	Pebble conglomerate	Upper plate, southern Saih Hatat	40Q 2584256/664059	Platy quartzite	13	1.7	2.1	1.7:1:0.47	0.6
DG98-138	Stretched pyrite	Upper plate, southern Saih Hatat	40Q 2586787/665407	Quartzite	3	2.2			
DG98-175	Criniod ossicles	Upper plate, Wadi Adai	40Q 2604157/654256	Limestone	8	1.3	1.3	1.28:1:0.8	1.0
DG98-185	Lithic fragments	NW side of Hatat bowl	40Q 2601569/647500	Hatat Schist	7	2.4			
DG98-185	Stretched pyrite	NW side of Hatat bowl	40Q 2601569/647500	Hatat Schist	1	1.8			
DG05-08	Lithic fragments (conglomerate)	SW side of Hatat bowl	40Q 2583185/642920	Hatat Schist	27	5.8	1.9	5.8:1:0.53	5.3
JM96-74	Hyaloclastite fragments	Huwl lower plate	40Q 259368/67399	Mafic Schist	31	2.2	6	2.2:1:0.2	0.2
JM96-77	Hyaloclastite fragments	Huwl lower plate	40Q 259347/67261	Metatuff	14	2.9	4.6	2.9:1:0.2	0.5
JM96-78	Hyaloclastite fragments	Huwl lower plate	40Q 259360/67237	Mafic schist	10	2.1	4.2	2.1:1:0.2	0.3
JM97-141	Pebble conglomerate	Beneath Hijam inlier, upper plate	40Q 260108/65991	Quartzite	30	1.7	2	1.7:1:0.5	0.7

n: sample size; *X*,*Y*,*Z*: maximum, intermediate and minimum principal strains; *k* is the Flinn strain ellipse shape value, where $k = (a-1)/(b-1)$ and $a = X/Y$ and $b = Y/Z$.

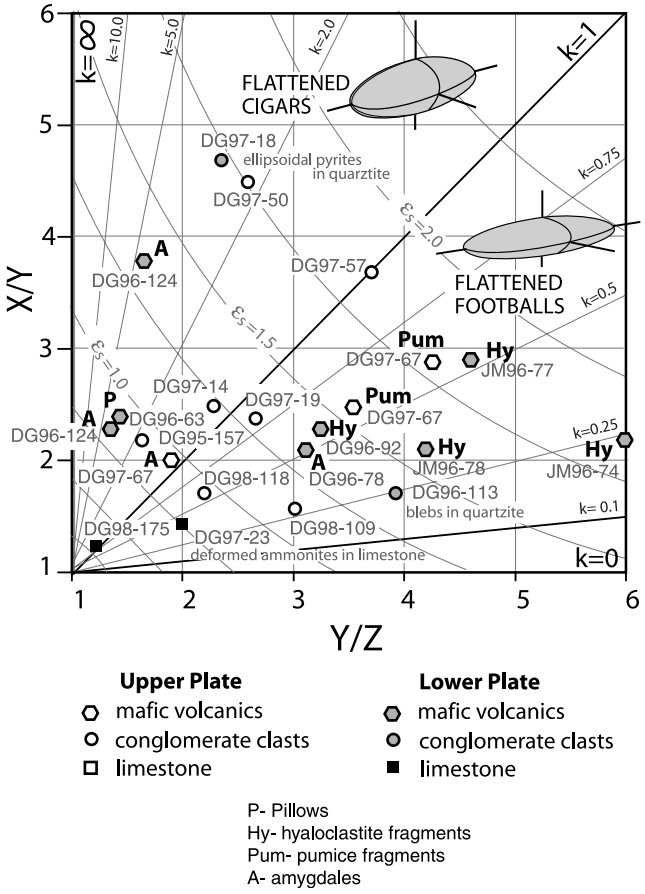

Fig. 11. Flinn strain plot showing both upper and lower plate total strain data (see Table 1). The graph has superimposed Flinn k value lines and Nadai octahedral shear strain contours (ε_s).

6.2. Strain variations

6.2.1. Lithology

Significant strain variations occur within different lithologies, in general with strain magnitudes in limestone > dolomite > calc-schist > quartz-mica schist > quartzite (see Tables 1 and 2).

For example, in the upper plate near the Hijam-Amdeh contact (DG97-95) pressure shadow strain determinations in quartzite gave $X/Z = 40{:}1$ ($n = 15$) with limestone at the same locality yielding $X/Z = 79.6$ ($n = 10$). In Wadi Huwl (lower plate locality DG96-85), pressure shadows in quartzite yielded an XZ strain of 6.9 ($n = 3$), whereas grey schist yielded XZ of 25:1 ($n = 10$). At locality DG96-69, pressure shadows yielded XZ strains of 42, 22, 9.7, 9 and 5.8 for limestone, limestone, calc-schist, quartzite and mafic schist, respectively (see Table 2). Also in the Huwl lower plate (locality DG96-90), quartz-mica schist with pressure shadows yielded an XY strain of 4.3 ($n = 15$, assuming plane strain), whereas pillows within a mafic schist adjacent to the quartz-mica schist yielded an XY strain of 2.5 ($n = 7$).

Total stretches determined from pressure shadows are always significantly greater than that determined from other markers in the same rock, in contrast to comparable strain determinations from different markers obtained by Durney (1972) from the Helvetic nappes. Deformed hyaloclastites containing pressure shadows provided comparative strain determinations (e.g. DG96-92) where an $X{:}Y{:}Z$ of 2.3:1:0.31 gives a X/Z strain ratio of 7.4, whereas the pressure shadows yielded an X/Z strain of 16.8 ($n = 10$, SD = 1.3). In Amdeh Quartzite (upper plate locality DG97-57), deformed pebble conglomerates yielded a $X{:}Y{:}Z$ of 3.7:1:0.27, which gives a X/Z strain of 13.7, whereas pressure shadows from an adjacent quartzite gave an XZ strain of 17.6.

6.2.2. Structural position

Measured strains are highest in the strongly deformed part of the upper plate immediately above the UP–LP shear zone (Figs. 7, 8b and 12b). There is a general gradient in strain towards this discontinuity (Fig. 7), as indicated previously (Miller et al., 1998). XZ strain data from pressure shadows (Table 2 and Fig. 12b) show lithology dependence as well as variation with structural proximity to the UP–LP shear zone.

Strain magnitude is variable in the lower plate with XZ strains ranging from 8:1 to 26:1 in mafic schist, with the largest XZ strain ratio of 228:1 recorded in calc-schist close to the folded UP–LP shear zone in the southern part of Wadi Huwl (Figs. 7, 8c and 12b). There is no apparent increase in strain upwards towards the UP–LP discontinuity. Lowest strains are recorded in the regional scale a-fold hinges. Strain markers were not obtained from the As Sheik and As Sifah shear zones.

XY strain data from total strain markers (Fig. 11a) are largely restricted to pebbles from Amdeh Quartzite conglomerates and to amygdales, hyaloclastite fragments and pillows in mafic schists, formerly mafic volcanic layers. The pebble strain data ranges from 1.6 to 4.5 (X/Y strain ratio) with the highest strain ratios in the immediate hanging wall to the UP–LP shear zone (Fig. 11a). Strain data from mafic volcanic layers in both the upper and lower plates range from 1.7 to 2.5 and do not seem to vary with position in the regional recumbent folds that occur within the lower plate.

6.3. Relationship to the lineation

In most instances, the lineation in the host rock matrix, defined either by calcite elongation in limestones and calc-mylonites or aligned phengites in mica schist and quartzites, is oblique to the stretch shown by markers such as pressure shadows on framboidal pyrites (see Fig. 7) and the long axes of deformed clasts in conglomerate units. There is commonly a deviation of some 10–15° from this direction in a clockwise sense, where the lineation has a more N-trend relative to the more NE-trend of the strain markers.

On the opposite limbs of major regional recumbent folds, this deviation changes to a counterclockwise sense, where

a. Total strain map— XY ellipses (in Sm)

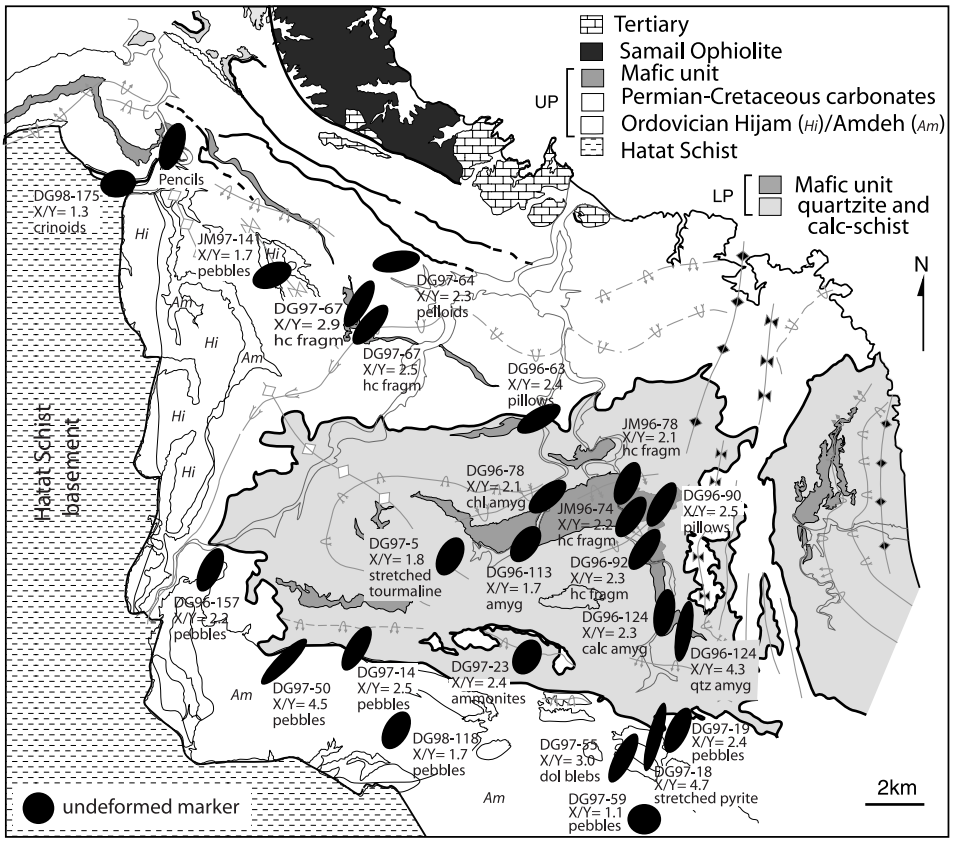

b. Total strain map— XZ ellipses from pressure shadows

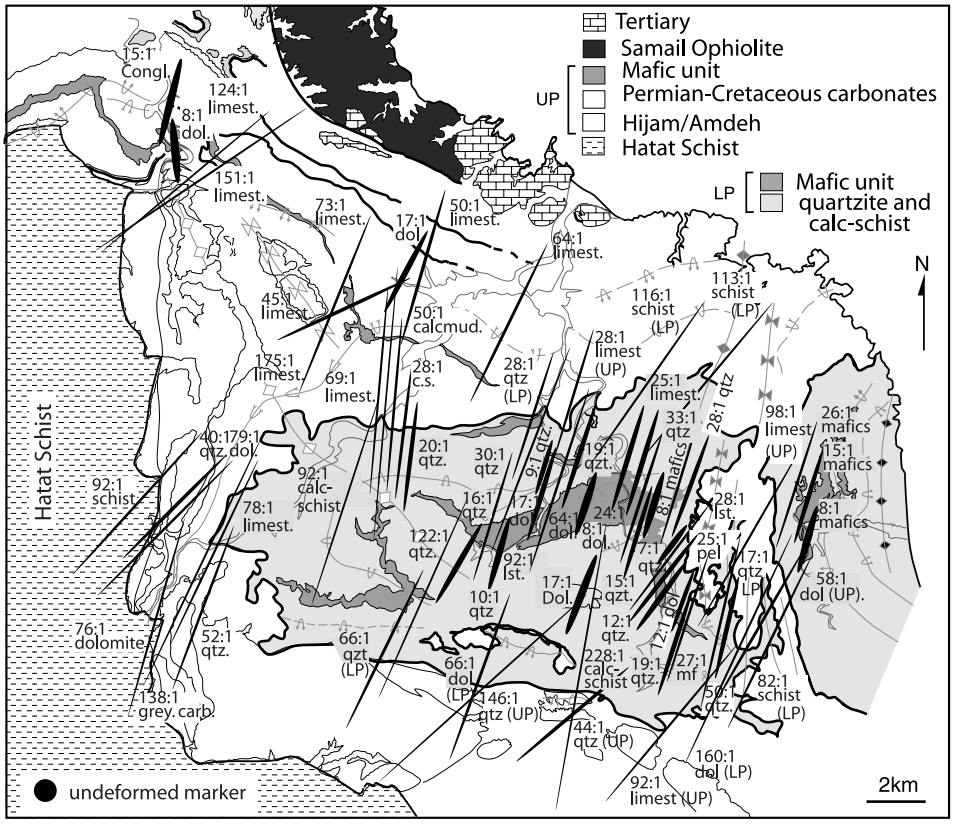

the lineation has a more NE-trend relative to the more N-trend of the strain markers (Fig. 12b). The amount of deviation remains the same.

7. Incremental strain markers

Incremental strain markers are predominantly pressure shadow fringes generally on pyrite (Table 2) within limestone, dolomite, calc-schist, quartz-mica schist and quartzite lithologies (Fig. 10). These all show an anti-taxial fibre growth where the youngest fibre growth segments are at the host pyrite interface (see Durney and Ramsay, 1973; Ramsay and Huber, 1983). Pressure shadow fringes have varying tail morphologies, ranging from undeformed, with recognisable fibres showing curvature and growth increments (Fig. 10A–D), to deformed, where fringes are long, straight and sometimes tapered, but generally lacking recognisable fibres (Fig. 10E). The latter, or deformed pressure shadows occur in calcite mylonites developed in upper plate Saiq 3 limestone in close proximity to the UP–LP shear zone and record very high total strain ($XZ > 100{:}1$). In thin section, however, most of the pressure shadow tails show effects of dynamic recrystallisation with tails made up of interlocking grains with undulose extinction and serrated grain boundaries, despite showing apparent fibrous form in hand specimen.

7.1. Fibre curvature

Fibre curvature varies in both the foliation and in the plane perpendicular to the foliation containing the lineation. In the plane of the schistosity, many pressure shadow fringes show a 20–30° change in fibre growth direction (Fig. 13). Most show a counterclockwise swing in the stretching direction within the schistosity plane. Initial increments exhibit an ENE or NE direction and the final increments are more N–S. This pattern is observed in both the strongly deformed upper plate samples (DG95-96, DG02-89, DG96-153 and DG96-50) as well as in the lower plate samples (DG96-80, DG96-74, DG96-127 and DG96-52; Fig. 13).

Some samples (DG96-80 and DG96-127) show similar rotational change but with a clockwise sense, but these occur on the opposite limbs of major recumbent folds to that of samples with counterclockwise increment rotation (Fig. 13). This once again supports the observations, particularly in Wadi Meeh gorge, that the lineation and pressure shadows have been folded around the regional recumbent hinges (Fig. 6c).

In the *XZ* plane, the movement plane normal to the foliation but parallel to the lineation, the pressure shadow fringes show curvatures reflecting a top-to-the-N or top-to-the-NE sense of shear (Fig. 10D). In most instances though, curvature of fibres in this plane appears to have been destroyed due to flattening elongation and associated dynamic recrystallisation and is only preserved with samples with lower overall total strain.

7.2. Timing of incremental stretch change

The lower bound for pressure shadow growth in the upper plate is that the stretching lineation and the pressure shadows are folded around the upper plate folds that show axial surface mica growth at ~70 Ma (Miller et al., 1999). Pressure shadows are also clearly deformed in mylonites of the UP–LP shear zone, which have yielded a mica Ar–Ar crystallisation age of ~76 Ma (Miller et al., 1999).

In the lower plate, pressure shadows are associated with fabrics formed in top-to-the-NE shear and containing a NE-trending stretching lineation. These fabrics have apparent Ar–Ar ages predominantly in the range of 100–78 Ma (Miller et al., 1999; Gray et al., 2004b).

8. Evolution of the fold-nappe

8.1. Key field and geochronological constraints

(1) The upper limb of the fold-nappe shows significantly lower penetrative strain, and macroscopic fold hinges are generally orthogonal to the regional NE–SW stretch direction.
(2) A consistent N- to NE-trending stretching lineation is defined by pressure shadows on framboidal pyrites, the long axes of deformed clasts in conglomerate units, mineral lineations defined by white mica, and more rarely by the long axes of pencils (Saiq 2v volcanics).
(3) A marked strain gradient into basal shear zone (upper plate–lower plate discontinuity); *X*/*Z* strain ratios change from ~16:1 to over 100:1 (where *X*, *Y* and *Z* are the maximum, intermediate and minimum principal stretches, respectively).
(4) Macroscopic regional folds have hinges parallel to the NE-trending regional/local stretching lineation approaching the basal high-strain zone.
(5) Pressure shadows are folded by these recumbent isoclines in both the upper and lower plates.
(6) Fibre curvature in pressure shadows in the foliation plane (*XY* plane) commonly shows a 20–30° increment rotation from ENE to NE or NNE.

Fig. 12. Strain maps of NE Saih Hatat showing the UP–LP discontinuity, the upper plate and Huwl and As Sifah lower plate windows. (a) *XY* strain map with black ellipses depicting strain magnitudes based on total strain determinations from conglomerate pebbles in Amdeh quartzite and pillows, hyaloclastite fragments and amygdules in mafic volcanics (see Table 1). (b) *XZ* strain map with *XZ* strain data superimposed onto map view. Black ellipses are based on *XZ* strains determined from pressure shadow fringes on pyrite (see Table 2). The criss-cross pattern of the strain ellipses reflects the change in orientation of both the stretching lineation and the strain marker principal stretch (*X*) direction due to folding around both minor and major folds.

Table 2
Strain data from pressure shadow fringes on pyrite

Field station	Location	Coordinates	Lithology	*n*	1+*e*	SD	*R*	*X* dirn
DG96-13 (*JM-96-6*)	Wadi Adai	40Q 260614/65584	Conglomerate	3	3.9	0.5	15	02/197
DG97-1 (JM97-1)	Wadi Adai	40Q 260519/65604	Dolomite	10	2.9	0.5	8	08/355
DG96-157 (*JM96-105*)	N–S wadi, E side Jabal al Khufaygi	40Q 259055/65700	Limestone	8	8.8	2.0	78	18/207
			Light grey carbonate	3	11.6	0.7	134	
DG96-156 (*JM96-105*)	N–S wadi, E side Jabal al Khufaygi	40Q 258927/65725	Amdeh quartzite	3	7.2	1.5	52	28/200
DG96-153 (*JM96-102*)	Hillside above Al Khufaygi	40Q 258864/65636	Dolomite	15	8.7	2.6	76	20/175
DG96-139 (*JM96-99*)	Side wadi off Wadi Meeh		Calc-mudstone	10	7.0	2.0	50	13/215
		40Q 259673/66458	Limestone	23	8.3	2.4	69	
			Dark-grey limestone	13	13.2	4.3	174	
DG96-141 (*JM96-101*)	Side wadi off Wadi Meeh	40Q 259598/66453	Calc-schist	5	5.3	1.9	28	14/190
			Quartzite	10	4.5	1.3	20	04/196
DG96-50 (*JM96-30*)	Wadi Huwl	40Q 259742/66978	Upper-plate limestone	7	5.3	1.6	28	32/348
DG96-52 (*JM96-32*)	Wadi Huwl	40Q 259676/66922	Lower-plate quartzite	9	5.3	0.8	28	11/048
DG96-69 (*JM96-39*)	Wadi Huwl	40Q 269563/66921	Lower-plate limestone	7	6.5	2.1	42	07/005
			Quartzite	8	3.0	0.9	9	
			Calc-schist	10	3.1	1.0	9	
			Mafic schist	9	2.4	1.1	6	
			Limestone	10	4.7	1.7	22	
DG96-75 (*JM96-36*)	Wadi Huwl (saddle b/w wadis)	40Q 259445/67029	Quartz-mica schist	11	4.3	1.5	19	20/210
			Dolomite	9	8.0	2.5	64	
DG96-74 (*JM96-40*)	Wadi Huwl	40Q 259445/67029	Quartzite	3	9.0	2.7	81	04/040
DG96-77 (*JM96-42*)	Wadi Huwl	40Q 259353/66921	Brown dolomite	4	3.1	0.5	10	18/023
			Silty dolomite	5	2.8	0.7	8	
			Brown dolomite	2	4.1	0.2	17	
DG96-80 (*JM96-40*)	Wadi Huwl	40Q 259243/67245	Quartzite	1	6.2	–	36	00/040
DG96-100	Wadi Huwl	40Q 259207/66855	Quartzite/ mafic schist	3	4.1	0.5	17	10/210
DG96-109	End of ridgeline, W of Wadi Huwl	40Q 259269/66766	Qtz layer in dolomite	11	5.4	1.7	29	16/200
DG96-103	Wadi Huwl, W branch	40Q 259182/66753	Quartzite	18	3.2	0.8	10	02/200
JM96-55	Wadi Huwl, E branch	40Q 259466/67207	Dolomite	11	4.9	1.1	24	10/034
			Limestone	10	5.1	1.3	26	
JM96-77	Ridge E of Wadi Huwl, E branch	40Q 259347/67261	Quartzite/tuffite	13	5.8	0.8	33	01/210
JM96-76	Ridge E of Wadi Huwl, E branch	40Q 259362/67322	Quartzite/tuffite	15	3.9	0.5	15	
JM96-74A	E–W wadi, E of Masail (Huwl)	40Q 259368/67399	Mafic schist	11	2.8	0.3	7.6	01/210
DG96-83 (*JM96-49*)	E–W wadi, E of Masail (Huwl)	40Q 259253/67311	Mafic schist	2	7.1	0.8	51	02/210
DG96-85 (*JM96-50*)	E–W wadi, E of Masail (Huwl)	40Q 259255/67335	Quartzite	3	2.6	0.8	7	12/208
			Grey schist	10	5.0	1.0	25	
DG96-86 (*JM96-51*)	Ridge E of Masail (Huwl)	40Q 259263/67391	Limestone/dolomite	12	5.3	1.9	28	18/210
DG96-90	E–W wadi, Masail (Huwl)	40Q 259341/67368	Quartzite/mafic schist	12	4.4	1.5	20	05/210
			Quartzite/mafic schist	12	5.3	1.3	28	
DG96-92	Wadi Huwl	40Q 259173/67311	Mafic schist	10	4.1	1.3	17	04/215
DG96-97	Ridge E of Wadi Huwl	40Q 259136/67415	Quartzite	9	3.5	0.7	12	02/200
DG96-165	Inlier W of wadi Huwl	40Q 259089/67124	Brown dolomite	5	4.1	1.6	17	00/025
DG96-116	Below UP klippe, E of wadi Huwl	40Q 259031/67431	Brown dolomite	2	3.5	0.1	12	28/205
DG96-121	Below UP klippe, E of Wadi Huwl	40Q 258939/67451	Quartz-mica schist	2	7.1	0.8	51	18/198
DG96-122	Below UP klippe, E of Wadi Huwl	40Q 258922/67435	Quartz-mica schist	4	4.1	1.2	17	24/205
DG96-124 (*JM96-83*)	E of Wadi Huwl	40Q 258925/67394	Mafic schist	8	5.2	1.1	27	05/185

DG96-127 (*JM96-84*)	Wadi Huwl, near Masail village	40Q 258904/67345	Quartzite	12	4.3	1.4	19	24/240
DG96-47 (*JM96-25C*)	Branch off upper Wadi As Sifah	40Q 259319/67815	Mafic schist	20	5.1	1.2	26	36/205
DG96-41 (*JM96-23Z*)	Upper Wadi As Sifah	40Q 259283/67848	Quartz-mica schist	4	3.8	0.5	15	10/210
DG96-41 (*JM96-23X*)	Upper Wadi As Sifah		As Sifah Mafic schist	6	2.9	0.5	8	
DG97-5 (*JM97-3b*)	Huwl lower plate, Wadi Shakari	40Q 259082/66678		1	4.0		16	32/210
DG97-7 (*JM97-7*)	Huwl lower plate (hinge of regional syncline)	40Q 258950/66496	Quartzite	10	11.0	2.4	122	65/204
DG97-13 (*JM97-11*)	Huwl lower plate (below upper plate contact)	40Q 258798/66336	Quartzite	8	8.1	1.0	66	34/206
DG97-19 (*JM97-16*)	Huwl lower plate (close to upper plate contact—road to Hamah)	40Q 258798/66336	Muddy dolomite sq1	11	8.1	1.1	66	42/220
			Limestone sq1	10	8.8	2.5	77	
DG97-20 (*JM97-17*)	Huwl upper plate (close to lower plate contact—top of ridge)	40Q 258601/67373	Limestone sq1	9	9.6	1.6	92	16/220
			Grey limestone sq1	10	10.6	3.0	112	
JM97-30	Zone between Huwl and As Sifah (lower plate)	40Q 258871/67598	Interbedded dolomite and quartzite	7	12.7	1.2	160	14/205
JM97-32	Zone between Huwl and As Sifah (lower plate)	40Q 258887/67693	Quartz-mica schist	10	9.1	2.4	82	10/206
JM97-45c	Zone between Huwl and As Sifah (upper plate)	40Q 258948/67653	Dolomite sq1	9	7.6	0.9	58	16/210
JM97-51	Zone between Huwl and As Sifah (upper plate)	40Q 259355/67647	Limestone sq1	6	9.9	1.3	98	34/210
JM97-57	Zone between Huwl and As Sifah (lower plate)	40Q 259373/67472	Quartz-mica schist	8	9.0	1.0	82	10/206
JM97-66b	Zone between Huwl and As Sifah (lower plate)	40Q 259340/67601	Quartz-mica schist	9	11.5	1.5	131	16/215
DG97-28	Amdeh, upper plate	40Q 2585982/670235	Quartzite	4	6.6	0.5	44	16/230
DG97-32	LP near UP–LP contact, N of Salil	40Q 258745/67011	Limestone/calc-schist	6	15.1	3.2	228	26/190
DG97-36	UP–LP shear zone, N of Salil	40Q 2587164/6668309	Quartzite	6	12.1	2.9	146	38/200
			Calc-schist	8	8.1	1.4	66	
DG97-57 (*JM97-73*)	Amdeh, upper plate	40Q 258368/675077	Thick-bedded quartzite	9	6.5	0.8	42	38/228
DG97-64 (*JM97-75*)	Wadi Meeh (campsite gully)	40Q 2602308/664165	Limestone Sq3L	8	7.1	0.5	50	02/016
DG97-66 (*JM97-76*)	Wadi Meeh (gully on lower limb of regional synclinal nappe)	40Q 2601880/662948	Dolomite Sq2b	19	4.1	1.2	17	08/028
DG97-67 (*JM97-77*)	Wadi Meeh (gully on lower limb of regional synclinal nappe—traverse towards hinge)	40Q 2601570/661719	Limestone Sq1L (*float*)	10	8.6	1.7	73	12/202
			Limestone Sq1L	8	5.2	0.5	28	
DG97-68 (*JM97-78*)	Wadi Meeh (gully on lower limb of regional synclinal nappe—traverse towards hinge, directly below Amdeh inlier)	40Q 260167/66148	Limestone Sq1L	7	6.7	0.8	45	02/245
			Limestone Sq1L	5	7.6	0.7	58	
			Limestone Sq1L	9	5.0	0.5	25	
DG97-71 (*JM97-80*)	Region between Wadi Meeh and Wadi Huwl	40Q 2599028/666208	Limestone Sq3L	9	8.0	0.6	64	06/206
DG97-95	Hijam ridge above Wadi Meeh gorge	40Q 2591579/656006	Limestone	10	8.9	1.9	79	06/042
			Quartzite	15	6.3	40		
JM97-87	Traverse from Wadi Huwl along upper plate contact towards As Sifah (lower plate)	40Q 259693/67209	Quartzite	10	6.1	0.8	37	07/032
JM97-90	Traverse from Wadi Huwl along upper plate contact towards As Sifah (lower plate)	40Q 259763/67375	Quartz-mica schist	10	10.8	1.5	116	02/035
JM97-92	Traverse from Wadi Huwl along upper plate contact towards As Sifah (lower plate)	40Q 259760/67507	Quartz-mica schist	7	10.6	1.7	113	09/040
JM97-102	Bandar Khayran area. Mahil infolded with Sq3 (upper plate)	40Q 259833/67674	Dolomite Sq3	9	11.2	1.3	125	00/313
JM97-107	Traverse along Amdeh (upper plate)	40Q 259409/65611	Hatat Schist	12	9.6	1.0	92	
JM97-115b	Traverse from Wadi Meeh towards Huwl (lower plate)	40Q 259311/66255	Calc-schist	12	9.6	1.1	92	02/198

Table 2 (*continued*)

Field station	Location	Coordinates	Lithology	n	$1+e$	SD	R	X dirn
JM97-126	Wadi Adai (upper plate)	40Q 260436/65713	Limestone Sq1L	8	12.3	1.6	151	35/056
JM97-127f	Wadi Adai (upper plate)	40Q 260467/65689	Silty dolomite Sq1L	7	11.2	2.5	124	15/050

n is the number of measurements; $1+e$ is the stretch, determined from pressure shadow fibres, given l0 is the pyrite diameter and l1 is the fibre length plus pyrite diameter (after Durney and Ramsay, 1973); SD is the standard deviation; $R=X/Z$, where X and Z are the maximum and minimum principal stretches (assuming plane strain and constant volume deformation). Note: the calculated strains are for relative comparison only; X dirn, plunge/plunge direction of pressure shadow fibres or stretching lineation in host rock.

(7) Fibre stretch direction is commonly oblique to the fabric or mineral stretching lineation.
(8) Pressure shadow fibres are deformed and recrystallised within the basal high-strain zone, which yielded an $^{40}Ar/^{39}Ar$ mica crystallisation age of ~76 Ma (Miller et al., 1999).
(9) Total strain data indicate apparent constriction to apparent flattening ($0.5<k<5$); objects have either flattened cigar or flattened rugby football shapes.
(10) Pressure shadow fibre tails in XZ sections are also generally long and straight, although those with slight curvature indicate top to the north shear sense.
(11) The pre-Ordovician Formations, including Hatat schist and the Hijam Dolomite and Amdeh Quartzite units, exposed in the centre of the Saih Hatat window represent the core of this regional anticlinal closure. The Hatat Schist is strongly deformed with transposition layering, and a well-developed lineation that parallels the regional Cretaceous lineation. Any pre-Permian deformation has been thoroughly overprinted by the Cretaceous event.
(12) Fabric development in the fold-nappe was at ~70 Ma (Miller et al., 1999) at the time of ophiolite emplacement onto the margin.
(13) These mica crystallisation ages are younger or the same as zircon fission track ages from the same region (Saddiqi et al., 1995).

8.2. Implications of strain data for fold-nappe development

Strain state data require approximately plane strain deformation with some constrictional as well as flattening components, and imply either convergent flow or a form of shear-related flow plus marked flattening, but clearly without significant elongation parallel to the strike of the margin or structural front (i.e. approximate plane strain with k values close to 1).

These data record the initial stages of shear zone development, pre-folding in the upper plate, as the markers are folded around the hinges of major folds and are deformed within the basal high-strain or mylonite zone (Fig. 6). The markers are deformed as part of the overall ductile top-to-the-NE shear strain gradient associated with the upper plate–lower plate shear zone.

The fibre curvature in pressure shadows denotes the chronological succession of stretching increments, where the observed changes in fibre curvature and the resultant stretch matches the changing stretch recorded by fabrics within the As Sifah lower plate mega-boudins (see Gray et al., 2004b). There is a change from ENE stretch recorded by the earliest fabrics preserved in the mega-boudins to a more NNE stretch developed during partial exhumation of the lower plate (Miller et al., 2002). The change in extension direction must, however, predate fold-nappe development,

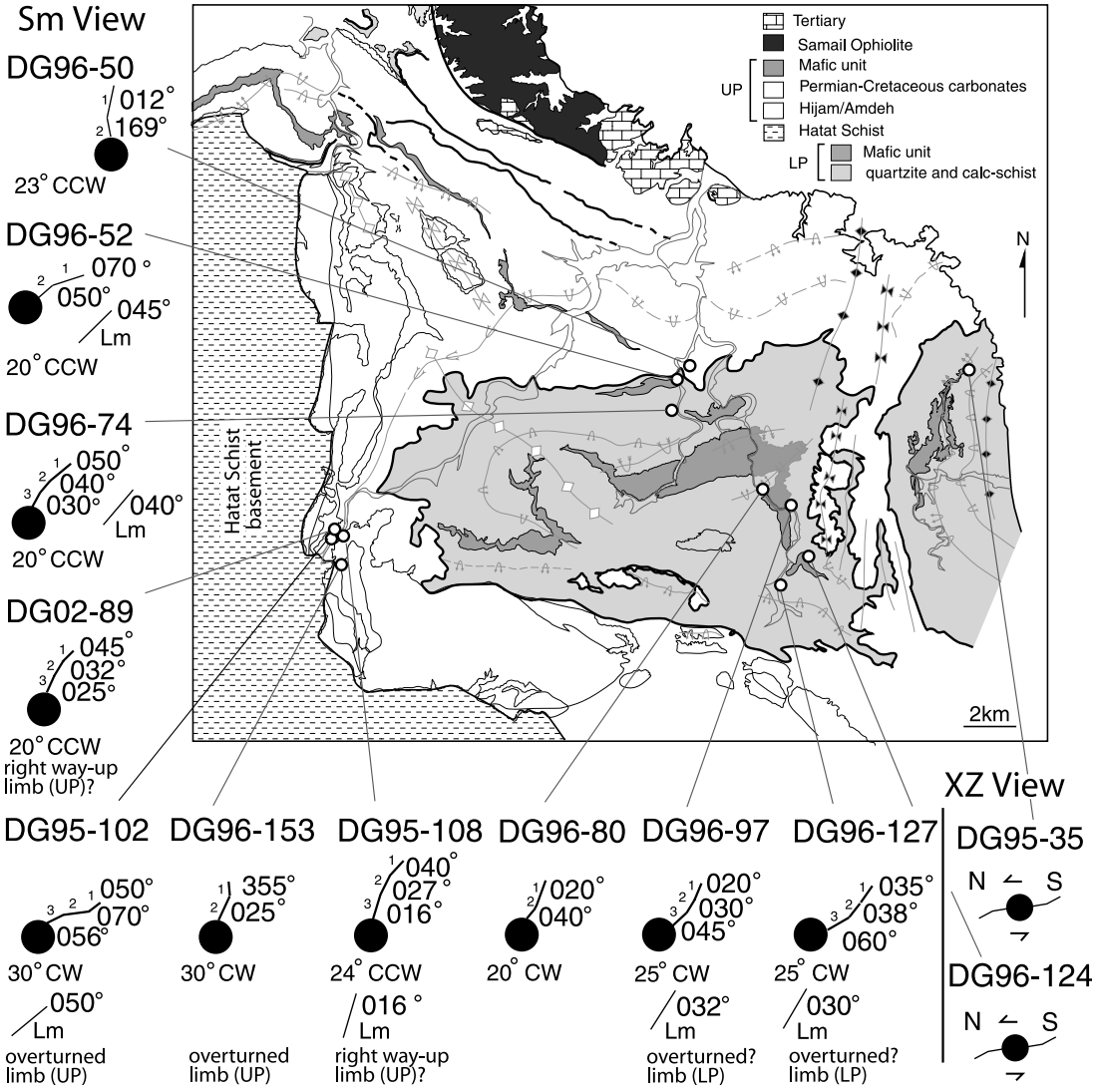

Fig. 13. Map of NE Saih Hatat showing fibre curvatures of pressure shadows in the foliation (or *XY* plane) at various localities in the upper and lower plates. Pressure shadow fibre increment changes are shown as bearings (0–360°), as well as the total stretch orientation change (in degrees) either in a clockwise (CW) or counterclockwise (CCW) sense. Two localities provide *XZ* views of fibre curvature (extreme right).

as pressure shadows with curved fibres are folded by major and minor folds in both the upper and lower plates.

8.3. Significance of structures and thermochronology of the lower plate

NE-directed shear fabrics within the lower part of the upper plate, the upper plate–lower plate shear zone and within the lower plate reflect a remarkable kinematic consistency, despite differences in timing of the deformation and metamorphism (Miller et al., 1998, 2002; Gray et al., 2004b).

The lower plate regional recumbent a- or x-type folds formed via intense, pervasive, NE-directed non-coaxial shear are associated with tiered top-to-the-NE shear zones (As Sheik and As Sifah shear zones in Fig. 7) that separate shear lenses or block with different *P–T–t* histories (cf. Miller et al., 1998, 2002). The As Sheik shear zone separates the Huwl and As Sifah units, largely exposed in their respective windows. Similar retrograde assemblages in the Huwl and As Sifah units suggest that the units attained similar crustal levels or were in similar metamorphic *P–T* space (Miller et al., 1999), prior to or during this intense top-to-the-NE shearing at 82–78 Ma (Miller et al., 1999, 2002; Gray et al., 2004a,b).

An apparent down-section increase in grade from the Huwl to the As Sifah units (Miller et al., 2002; Breton et al., 2004; Searle et al., 2004) suggests that the As Sheik shear zone has a ‘normal’ movement sense with either extensional character or as the bounding fault along the top of an upward moving block (Miller et al., 2002). It is interesting to note that this shearing event took place while high-*P* metamorphism was still occurring in the lower plate as shear sense indicators are either defined by high-Si phengite or

overgrown by later sodic amphibole (Miller et al., 1999; Gray et al., 2004a,b).

Juxtaposition of upper and lower plates is characterised by development of metamorphic disequilibrium assemblages in the lower plate schists close to the UP–LP contact (Goffé et al., 1988; Miller et al., 1998, 1999, 2002). These schists record partial resetting of argon in phengite lattices with disturbed $^{40}Ar/^{39}Ar$ spectra at ~74 Ma (Miller et al., 1999, 2002; Gray et al., 2004a,b).

8.4. Significance of UP–LP shear zone

The variation in structural style of the upper plate with deeper structural level suggests that the upper–lower plate discontinuity has a direct control on the deformation of the upper plate (Miller et al., 2002). The increase in strain, the highly attenuated or thinned stratigraphy and the development of shear-related flattening fabrics, as well as mylonitic fabrics that merge with and are subparallel to the UP–LP shear zone all suggest shear-related deformation in the lower levels of the upper plate linked to shear displacement along the reactivated UP–LP shear zone.

8.5. Saih Hatat fold-nappe evolution—a summary

Strain magnitude and kinematic considerations require development of the major Saih Hatat fold-nappe beneath the Samail Ophiolite nappe (Fig. 14) to involve:

(1) initial truncation of upper plate stratigraphy with hanging wall cut-off relationships dictating a dip on the fault/shear zone toward the craton;
(2) NE-directed shear strain and shear displacement along this shear zone with development of a marked strain gradient in the upper plate;
(3) subsequent fold-nappe development in the hanging wall (upper plate) to this shear zone due to continued NE-directed shear.
(4) the upper limb is effectively pinned to the autochthon requiring accumulation of NE-directed shear strain largely by movement of the lower plate to the SW.
(5) nappe development involves a ‘rolling hinge’ where the upper limb cycles through the hinge into a zone of intense shear strain on the fold lower limb (suggested by folding of the L–S tectonite or mylonitic fabric and strain markers by major upper plate folds), and
(6) a component of shear-related flattening (suggested by marked shortening in the Hatat Schist in the core of the fold-nappe).

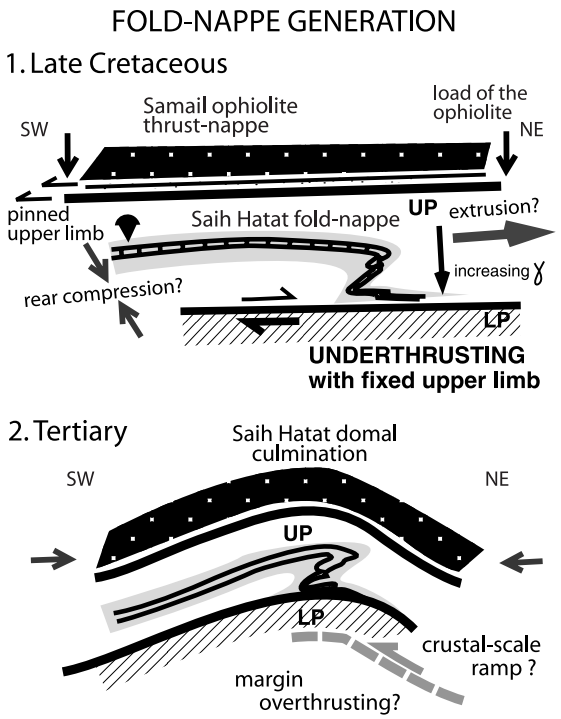

Fig. 14. Schematic diagram summarising Saih Hatat fold-nappe evolution showing (1) the inferred mechanisms responsible for the Late Cretaceous fold-nappe, and (2) the present day geometry based on Tertiary evolution of the domal culmination. For simplicity the UP–LP shear zone has been drawn as horizontal. The dominant mechanism to form the fold-nappe is underthrusting by the lower plate (LP) causing differential shear strain in the upper plate (UP). The Saih Hatat fold-nappe forms due to the combined effects of pinning of the upper plate stratigraphy to the autochthon, a mechanical stratigraphy, and intense NE-directed shear strain through the upper plate. Other possible, but less likely effects are from the load of the ophiolite causing a form of rear compression and/or extrusion.

9. Mechanism of fold-nappe formation—a discussion

Large-scale recumbent fold formation has been attributed to several mechanisms, including over-folding into over-thrusting after Heim (1919, in Merle, 1998), gravitational spreading analogous to glacier flow, extruding spreading involving rear compression and extrusion of cover attendant with deformation of basement, along with variants such as spreading-gliding (see fig. 39 of Merle, 1998).

The development of fold-nappes involving the fold-pair mechanism after Heim (1919, cited in Merle, 1998) requires firstly that the over-folding predates the development of the shear zone along the common limb, and secondly that the oppositely closing hinges in the hanging wall and footwall to the shear zone, respectively, must involve the same stratigraphy (see fig. 4 of Merle, 1998). Neither situation holds for the Saih Hatat fold-nappe, as the fold-nappe clearly postdates the shear zone, and the shear zone does not have the same stratigraphy in the hanging wall relative to the footwall (see Miller et al., 2002, p. 363; Gray et al., in press).

General spreading by gravitational-induced flow requires a decrease in the strain magnitude towards the rear of the nappe due to decreased shear displacement (fig. 40 of Merle, 1998). This model involves a frontal rolling hinge (e.g. Merle, 1998, fig. 17), but the resultant strain pattern

has distinct differences to that observed in the Saih Hatat fold-nappe. The increase in strain magnitude towards the UP–LP shear zones is suggestive of a component of gliding due to ductile flow in the lower part of the fold-nappe (i.e. gliding-spreading), but as the Saih Hatat fold-nappe must have been constrained above by the Samail Ophiolite thrust-nappe and below by the lower plate, it would appear that some form of extrusion also has to be involved.

Extruding spreading of sedimentary cover occurs after shortening in the basement, with extrusion of the cover units from a root zone involving rear compression (e.g. nappes of the Helvetic Alps). Rear compression is reflected by an increase in the intensity of deformation towards the rear of the nappe (e.g. Merle, 1998, figs. 39 and 51), but this is not seen in Saih Hatat and there is no apparent root zone. The pre-Ordovician Hatat Schist (basement) is clearly deformed due to deformation that has affected the upper plate during the fold-nappe formation. Lineations and foliation are similar across the boundary between the basement and the unconformably overlying units (e.g. Hijam and Amdeh units) (see Miller et al., 2002). The similarity in deformational style of the basement and the sedimentary cover was first noted by Michard et al. (1984), but they argued for SW-directed shearing during schistosity development. The Hatat Schist deformation represents shear-related tightening of the fold-nappe possibly incorporating a load component from the overlying ophiolite.

The Saih Hatat fold-nappe strain pattern reflects increased ductile strain due to NE-directed shear towards the controlling upper plate–lower plate shear zone. Fold-nappe development was by a frontal rolling mechanism during increased NE-directed shear strain in the upper plate, causing folding of the earlier formed high-strain fabrics and intense, shear-related flattening deformation in the Hatat Schist (basement) (cf. Ramsay et al., 1983; Dietrich and Casey, 1989). The presence of the overlying ophiolite sheet precludes the influence of all forms of gravitationally induced spreading in fold-nappe development.

9.1. Geodynamical significance

The structural, kinematic and geochronological data presented and/or discussed in this paper require a three-stage evolution to produce the upper crustal geometry preserved in the Saih Hatat domal culmination. This involves (1) partial exhumation of the lower plate to mid-crustal levels by ~78 Ma (Miller et al., 1998, 1999, 2002), in a manner not too dissimilar to that proposed by Chemenda et al. (1996); followed by (2) continued convergence and reburial of the lower plate with emplacement of the ophiolite onto the margin, and (3) final development of the Saih Hatat fold-nappe between ~76 and 70 Ma as a response to loading instability by the ophiolite analagous to an antithetic backfold (cf. Escher and Beaumont, 1997) or form of retrocharriage (see Roeder, 1977). Fold-nappe development occurred when the ophiolite thrust-nappe formed a 'lid' to the developing tectonic wedge on the leading edge of the Arabian margin (cf. Miller et al., 2002). Stratigraphic and sedimentologic data suggest that the ophiolite thrust-nappe had encountered the Arabian margin by ~80 Ma (Warbuton et al., 1990).

10. Conclusions

Recumbent folding of bedding, transposed layering and mylonitic layering containing a stretching lineation and pressure shadow fringes on pyrite record the development of a major NE-facing recumbent fold-nappe beneath the Samail Ophiolite on the NE Arabian Peninsula. Strain markers provide a relative measure of strain variation through the fold-nappe and show a marked increase in strain towards a major shear zone (UP–LP shear zone) at its base. Markers with initial spheroidal shapes (e.g. amygdales in mafic volcanics) indicate approximate plane strain to constrictional deformation.

Folding of the strain markers and the earlier formed high-strain fabrics to form the fold-nappe requires a frontal rolling mechanism operative during top-to-the-NE shear. The pinning of the upper limb to the autochthon and the inferred relative movements of lower plate crustal units in the footwall suggest that Saih Hatat fold-nappe kinematic evolution simply involves underthrusting by movement of the footwall relative to a stationary hanging wall. The fold-nappe therefore develops due to hanging wall differential shear strain and a mechanical stratigraphy. There is no evidence of gravitationally induced spreading in fold-nappe development.

Acknowledgement

Funding for the research was from Australian Research Council grants (Monash U. 95 Small Grant, ARC Large Grant A39601548 and an ARC Discovery Grant DP0210178 awarded to DRG), and a National Science Foundation Grant EAR91-06016 (awarded to RTG). Miller was supported by a Monash University Graduate Scholarship (1995–1998). We thank Dr Hilal Al Azry (Director General of Minerals) and Dr Salim Hamed Al Busaidi (Director of Oman Geological Survey) for sponsorship and support during the fieldwork, Jean-Paul Breton (Resident Director, B.R.G.M. Oman) and Jack Filbrandt (PDO) for some logistical support and discussions on aspects of Oman geology and Mark Jessell for producing the false colour Landsat image in Fig. 3. We acknowledge reviews by Olivier Merle and Jean-Paul Breton, and thank Jean-Paul for an incredibly detailed critique that forced us to refocus the manuscript.

References

Alleman, F., Peters, T., 1972. The ophiolite–radiolarite belt of the northern Oman Mountains. Eclogae geologisch Helvetia 65, 657–697.

Bailey, E.H., 1981. Geological map of the Muscat-Ibra area, Sultanate of Oman. Journal of Geophysical Research 86. B4 pocket map.

Béchennec, F., Le Métour, J., Rabu, D., Bourdillon-de-Grisac, Ch., De Wever, P., Beurrier, M., Villey, M., 1990. The Hawasina Nappes: stratigraphy, palaeogeography and structural evolution of a fragment of the south-tethyan passive continental margin. In: Robertson, A.H., Searle, M.P., Ries, A.C. (Eds.), The Geology and Tectonics of the Oman Region Geological Society of London Special Publication, 49, pp. 213–223.

Bertrand, M., 1844. Rapport du structure des Alpes de Glaris et du basin Houllier du Nord. Bull. Soc. Geol. France 12, 318–330.

Breton, J.P., Béchennec, F., Le Métour, J., Moen-Morel, L., Razin, P., 2004. Eoalpine (Cretaceous) evolution of the Oman Tethyan continental margin: insights from a structural study in Jabal Akhdar (Oman Mountains). GeoArabia 9, 1–18.

Cawood, P.A., Green, F.K., Calon, T.J., 1990. Origin of Culminations within the Southeast Oman Mountains at Jebel Ma Jhool and Ibra Dome. In: Robertson, A.H.F., Searle, M.P., Ries, A.C. (Eds.), The Geology and Tectonics of the Oman Region Geological Society of London Special Publication, 49, pp. 429–446.

Chemenda, A.I., Mattauer, M., Bokun, A.N., 1996. Continental subduction and a mechanism for exhumation of high-pressure metamorphic rocks: new modelling and field data from Oman. Earth and Planetary Science Letters 143, 173–182.

Dietrich, D., Casey, M., 1989. A new tectonic model for the Helvetic nappes. In: Coward, M.P., Dietrich, D., Park, R.G. (Eds.), Alpine Tectonics Geological Society of London Special Publication, 45, pp. 47–63.

Dietrich, D., Durney, D.W., 1986. Change of direction of overthrust shear in the Helvetic nappes of western Switzerland. Journal of Structural Geology 8, 389–398.

Durney, D.W., 1972. Deformation history of the western Helvetic nappes, Valais, Switzerland. Unpublished PhD Thesis, Imperial College, London.

Durney, D.W., Ramsay, J.G., 1973. Incremental strains measured by syntectonic crystal growth. In: Dejong, K., Scholten, R. (Eds.), Gravity and Tectonics. Wiley, New York.

El-Shazly, A.K., 1994. Petrology of lawsonite-, pumpellyite- and sodic amphibole-bearing metabasites from NE Oman. Journal of Metamorphic Geology 12, 23–48.

El-Shazly, A.K., 1995. Petrology of Fe–Mg–carpholite-bearing metasediments from NE Oman. Journal of Metamorphic Geology 13, 379–396.

El-Shazly, A.K., Coleman, R.G., 1990. Metamorphism in the Oman Mountains in relation to the Semail ophiolite emplacement. In: Robertson, A.H., Searle, M.P., Ries, A.C. (Eds.), The Geology and Tectonics of the Oman Region Geological Society of London Special Publication, 49, pp. 473–493.

Escher, A., Beaumont, C., 1997. Formation, burial and exhumation of basement nappes at crustal scale: a geometric model based on the Western Swiss–Italian Alps. Journal of Structural Geology 19, 955–974.

Flinn, D., 1962. On folding during three dimensional progressive deformation. Quarterly Journal of the Geological Society 118, 385–433.

Glennie, K.W., Hughes Clarke, M.W., Boeuf, M.G., Pilaar, W.F., Reinhardt, B.M., 1974. Geology of the Oman Mountains. Verhandelingen van het Koninklinjk Nederlands geolgisch minjbouwkundig Genootsschap, Amsterdam 31, 423pp.

Goffé, B., Michard, A., Kienast, J.R., Le Mer, O., 1988. A case of obduction-related high pressure, low temperature metamorphism in upper crustal nappes, Arabian continental margin, Oman. Tectonophysics 151, 363–386.

Gray, D.R., Gregory, R.T., 2003. Ophiolite obduction and the Samail Ophiolite: the behaviour of the underlying margin. In: Dilek, Y., Robinson, P.T. (Eds.), Ophiolites and Earth History Geological Society of London Special Publication, 218, pp. 449–466.

Gray, D.R., Gregory, R.T., Miller, J.Mc., 2000. A new structural profile along the Muscat-Ibra transect, Oman: implications for the emplacement of the Samail Ophiolite. In: Dilek, Y., Moores, E.M., Elthon, D., Nicolas, A. (Eds.), Ophiolites and Oceanic Crust: New Insights from Field Studies and the Ocean Drilling Program Geological Society of America Special Paper, 349, pp. 513–523.

Gray, D.R., Hand, M., Mawby, J., Armstrong, R.A., Miller, J.McL., Gregory, R.T., 2004a. Sm–Nd and zircon U–Pb ages from garnet-bearing eclogites, NE Oman: constraints on high-P metamorphism. Earth and Planetary Science Letters 222, 402–422.

Gray, D.R., Miller, J.McL., Foster, D.A., Gregory, R.T., 2004b. Transition from subduction- to exhumation-related fabrics in glaucophane-bearing eclogites, Oman: evidence from relative fabric chronology and $^{40}Ar/^{39}Ar$ ages. Tectonophysics 389, 35–64.

Gray, D.R., Gregory, R.T., Armstrong, R.A., Miller, J.McL., Richards, I., in press. Age and stratigraphic relationships of structurally deepest level rocks, Oman Mountains: U–Pb SHRIMP evidence for Late Carboniferous Neo-Tethys rifting. Journal of Geology.

Gregory, R.T., Gray, D.R., Miller, J.McL., 1998. Tectonics of the Arabian Margin associated with the emplacement of the Oman Margin along the Ibra Transect: new evidence from NE Saih Hatat. Tectonics 17, 657–670.

Hanna, S., 1990. The Alpine deformation of the Central Oman Mountains. In: Robertson, A.H.F., Searle, M.P., Ries, A.C. (Eds.), The Geology and Tectonics of the Oman Region Geological Society of London Special Publication, 49, pp. 341–359.

Le Métour, J., de Gramont, X., Villey, M., 1986. Geological map of Masqat and Quryat, sheets NF40-4A, NF40-4D, scale 1:100,000. Explanatory notes. Ministry of Petroleum and Minerals, Directorate General of Minerals, Sultanate of Oman.

Le Métour, J., Rabu, D., Tegyey, M., Béchennec, F., Beurrier, M., Villey, M., 1990. Subduction and obduction: two stages in the Eo-Alpine tectonometamorphic evolution of the Oman Mountains. In: Robertson, A.H., Searle, M.P., Ries, A.C. (Eds.), The Geology and Tectonics of the Oman Region Geological Society of London Special Publication, 49, pp. 327–339.

Lippard, S.J., Shelton, A.W., Gass, I.G., 1986. The ophiolite of northern Oman. Geological Society of London, Memoir 11.

Mann, A., Hanna, S.S., 1990. The tectonic evolution of pre-Permian rocks, Central and Southeastern Oman Mountains. In: Robertson, A.H., Searle, M.P., Ries, A.C. (Eds.), The Geology and Tectonics of the Oman Region. Geological Society of London Special Publication, 49, pp. 307–325.

Mattauer, M., Ritz, J.-F., 1996. Arguments géologiques en faveur d'un modèle de subduction continentale pour l'exhumation du metamorphisme haute-pression d'Oman. Centre Rendue Acadamie des Sciences Paris, série IIa 322, 869–876.

Merle, O., 1998. Emplacement Mechanisms of Nappes and Thrust Sheets. Kluwer Academic Publishers, Dordrecht, The Netherlands. 158pp.

Michard, A., Bouchez, J.L., Ouazzani-Touhami, M., 1984. Obduction related planar and linear fabrics. Journal of Structural Geology 6, 39–49.

Michard, A., Goffé, B., Saddiqi, O., Oberhänsli, R., Wendt, A.S., 1994. Late Cretaceous exhumation of the Oman blueschists and eclogites: a two stage extensional mechanism. Terra Nova 6, 404–413.

Miller, J.McL., Gray, D.R., Gregory, R.T., 1998. Exhumation of high-pressure rocks, northeastern Oman. Geology 26, 235–238.

Miller, J.McL., Gray, D.R., Gregory, R.T., 1999. Geological and geochronological constraints on the exhumation of a high-pressure metamorphic terrane, Oman. In: Ring, U., Brandon, M.T., Lister, G.S., Willet, S.D. (Eds.), Exhumation Processes: Normal Faulting, Ductile Flow and Erosion Geological Society, London, Special Publication, 154, pp. 241–260.

Miller, J.McL., Gray, D.R., Gregory, R.T., 2002. Geometry and significance of internal windows and regional isoclinal folds in northeast Saih Hatat, Sultanate of Oman. Journal of Structural Geology 24, 359–386.

Mount, V.S., Crawford, R.I.S., Bergman, S.C., 1998. Regional structural style of the Central and Southern Oman Mountains: Jabal Akhdar, Saih Hatat, and the Northern Ghaba Basin. GeoArabia 3, 475–490.

Nadai, A., 1963. Theory of Fracture and Flow of Solids—Engineering Societies Monograph. McGraw-Hill, New York. 705pp.

Ramsay, J.G., Huber, M.I., 1983. The Techniques of Modern Structural Geology, Strain Analysis, vol. 1. Academic Press, London. 307pp.

Ramsay, J.G., Casey, M., Kligfield, R., 1983. Role of shear in development of the Helvetic-fold-thrust belt of Switzerland. Geology 11, 439–442.

Roeder, D., 1977. Continental convergence in the Alps. Tectonophysics 40, 339–350.

Saddiqi, O., Poupeau, G., Michard, A., Goffé, B., Oberhänsli, R., 1995. Exhumation des roches métamorphiques HP–BT d'Oman: datation par traces de fission sur zircons. Comptes Rendus de l'Académie des Sciences, Paris 320 (IIa), 1071–1077.

Searle, M.P., 1985. Sequence of thrusting and origin of culminations in the northern and central Oman Mountains. Journal of Structural Geology 7, 129–143.

Searle, M.P., Cox, J., 1999. Tectonic setting, origin and obduction of the Oman Ophiolite. Geological Society of America Bulletin 111, 104–122.

Searle, M.P., Waters, D.J., Martin, H.N., Rex, D.C., 1994. Structure and metamorphism of blueschist-eclogite facies rocks from the NE Oman Mountains. Journal of the Geological Society, London 151, 555–576.

Searle, M.P., Warren, C.J., Waters, D.J., Parrish, R.R., 2004. Structural evolution, metamorphism and restoration of the Arabian continental margin, Saih Hatat region, Oman Mountains. Journal of Structural Geology 26, 451–473.

Warbuton, J., Burnhill, T.J., Graham, R.H., Isaac, K.P., 1990. The evolution of the Oman Mountains Foreland basin. In: Robertson, A.H., Searle, M.P., Ries, A.C. (Eds.), The Geology and Tectonics of the Oman Region Geological Society of London Special Publication, 49, pp. 419–427.